Positivity-preserving and symmetry-preserving Lagrangian schemes for compressible Euler equations in cylindrical coordinates

Dan Ling[1], Juan Cheng[2] and Chi-Wang Shu[3]

Abstract

For a Lagrangian scheme solving the compressible Euler equations in cylindrical coordinates, two important issues are whether the scheme can maintain spherical symmetry (symmetry-preserving) and whether the scheme can maintain positivity of density and internal energy (positivity-preserving). While there were previous results in the literature either for symmetry-preserving in the cylindrical coordinates or for positivity-preserving in cartesian coordinates, the design of a Lagrangian scheme in cylindrical coordinates, which is high order in one-dimension and second order in two-dimensions, and can maintain both spherical symmetry-preservation and positivity-preservation simultaneously, is challenging. In this paper we design such a Lagrangian scheme and provide numerical results to demonstrate its good behavior.

Keywords: Lagrangian method; cylindrical coordinates; symmetry-preserving; positivity-preserving; compressible flows

[1]Graduate School, China Academy of Engineering Physics, Beijing 100088, China. E-mail: lingdan189@126.com. Research is supported in part by Science Challenge Project. No. JCKY2016212A502.

[2]Institute of Applied Physics and Computational Mathematics, Beijing 100088, China. E-mail: cheng_juan@iapcm.ac.cn. Research is supported in part by NSFC grants 11471049 and U1630247 and Science Challenge Project. No. JCKY2016212A502.

[3]Division of Applied Mathematics, Brown University, Providence, RI 02912. E-mail: shu@dam.brown.edu. Research is supported in part by ARO grant W911NF-15-1-0226 and NSF grant DMS-1418750.

1 Introduction

There are two different and typical frameworks to describe the motion of fluid flow, namely the Eulerian framework and the Lagrangian framework. When we mention the latter framework, we refer to the kinematic description which considers a time dependent reference frame that follows the fluid motion. Lagrangian methods are more suitable for problems involving interfaces between materials or free surfaces and are widely applied in many fields of multi-material flow simulations such as in astrophysics or in inertial confinement fusion (ICF).

In these applications, there often exist spherical-symmetric models such as sphere-shape capsules. When such models are simulated by Lagrangian methods in cylindrical coordinates, it is a critical and challenging issue to preserve the spherical symmetry in the cylindrical coordinate system which is distinct from that symmetry. For example, in the simulation of an implosion problem with strong compressions, the preservation of spherical symmetry is very important, since the small deviation from spherical symmetry due to numerical errors may be amplified by Rayleigh-Taylor or other instabilities which may potentially produce unpredictably large errors. Earlier strategies to design schemes in two-dimensional cylindrical coordinates to preserve spherical symmetry often sacrifice momentum and energy conservation, or at least momentum conservation. In [3], a cell-centered Lagrangian scheme was developed based on the control volume discretization. By discretizing the source term in the momentum equation compatibly, the scheme was designed to preserve one-dimensional spherical symmetry in a two-dimensional cylindrical geometry using an equal-angel-zoned grid without losing conservation. Based on the first order control volume scheme of Maire in [12], Cheng and Shu applied the methodology in [3] to obtain the spherical symmetry property. This modified scheme can keep several good properties, such as symmetry, conservation and the geometric conservation law (GCL). In order to get higher than first-order symmetry-preserving schemes, Cheng and Shu in [6] presented a second-order cell-centered Lagrangian scheme for solving Euler equations of compressible gas dynamics in cylindrical

coordinates. This scheme not only preserves symmetry but also preserves the conservation for mass, momentum and total energy as well as the GCL.

Another important issue in computational fluid dynamics is the positivity-preserving property. As in a conservative approximation to Euler equations where density, momentum and total energy are solved directly, the kinetic energy is computed from mass and momentum and then subtracted from the total energy to provide internal energy. Therefore, at high Mach numbers, the internal energy appears as a small difference of two large quantities, and is prone to large percentage errors. It may easily become negative numerically which may lead to nonlinear instability and a failure of the numerical scheme. To overcome this difficulty, many first order positivity-preserving Eulerian schemes were developed in earlier years, for instance, the classical Godunov scheme [8], Lax-Friedrichs scheme [16, 20], the modified HLLE scheme [8] and the HLLC scheme [1] and so on. Some of them are designed also up to second order accuracy. Recently, Zhang and Shu proposed a general framework of high-order positivity-preserving Eulerian schemes such as the Runge-Kutta discontinuous Galerkin (RKDG) methods and the weighted essentially non-oscillatory (WENO) finite volume schemes in [20, 21, 22].

Compared with Eulerian methods, positivity-preserving Lagrangian schemes are less investigated. The pioneering work on this issue includes the positivity-preserving Godunov-type scheme based on the modified HLL Riemann solver [14], and the positive and entropic schemes [9]. In [5], Cheng and Shu constructed high order positivity-preserving Lagrangian schemes in one- and in two-dimensional spaces by developing an HLLC Riemann solver and applying the Zhang-Shu positivity-preserving framework. More recently, cell-centered high order positivity-preserving Lagrangian schemes for compressible flows in both one-dimensional and two-dimensional spaces were presented by Vilar et al in [18, 19] relying on the two-state solver. We remark that these schemes are designed in cartesian coordinates and for problems without source terms. For equations in non-cartesian coordinates and with source terms, positivity-preserving is more difficult to achieve. This is especially the case

when symmetry-preserving must also be taken into consideration.

In this paper, we will focus on designing high order cell-centered Lagrangian schemes which can achieve positivity-preserving and symmetry-preserving properties simultaneously. This is not a straightforward combination of the symmetry-preserving technique in [3, 6] and the positivity-preserving technique in [5, 18, 19], since the design of one technique must ensure that the other property is not lost. In the one-dimensional case, for the positivity-preserving property, we make an additional time step constraint by controlling the change rate of the control volume to achieve this goal with any definition of positive acoustic impedance, mainly following [5, 18, 19, 21]. For the extension to two-dimensions, the design and analysis are similar, however the positivity-preserving limiter must be carefully applied in order not to affect the spherical symmetry preservation when computed on an equal-angle-zoned grid. For this purpose, our scheme is based on the work of Cheng and Shu in [6] and makes a careful balance between the original symmetry-preserving framework and the new positivity-preserving modification, in order to make sure one does not affect the performance of the other. The final scheme thus has both symmetry-preserving and positivity-preserving properties, as well as the GCL and conservation properties.

The remainder of this paper is organized as follows: In Section 2, we first formulate the compressible Euler equations in cylindrical coordinates, describe the two-state Riemann solver, and then design the first order and high order positivity-preserving Lagrangian schemes in this one-dimensional case. In Section 3, we show how to extend the positivity-preserving technique to two-dimensional cylindrical coordinates without destroying the original spherical symmetry preservation. In Section 4, one- and two-dimensional numerical examples are given to verify the performance of our positivity-preserving and symmetry-preserving Lagrangian schemes. In Section 5, we will make some concluding remarks.

2 One-dimensional case

The Euler equations for gas dynamics in one-dimensional cylindrical coordinates can be given by the following integral form in the Lagrangian framework

$$\begin{cases} \dfrac{d}{dt}\displaystyle\int_{\Omega(t)} \rho r dr = 0, \\ \dfrac{d}{dt}\displaystyle\int_{\Omega(t)} \rho u r dr = -(rp)|_{\Gamma_r(t)} + (rp)|_{\Gamma_l(t)} + \int_{\Omega(t)} p dr, \\ \dfrac{d}{dt}\displaystyle\int_{\Omega(t)} \rho E r dr = -(rpu)|_{\Gamma_r(t)} + (rpu)|_{\Gamma_l(t)} \end{cases} \tag{2.1}$$

where $r > 0$ denotes the radial direction, ρ is density, u is velocity, p is pressure and E is specific total energy, $\Gamma_l(t)$ and $\Gamma_r(t)$ are the left and right boundaries of the control volume $\Omega(t)$. The system (2.1) presents the conservation of mass, momentum and total energy.

The set of equations is completed by the additional equation of state (EOS), which has the following general form

$$p = p(\rho, e),$$

with the specific internal energy $e = E - \frac{1}{2}u^2$. The thermodynamic sound speed for the fluid flow is defined as $a^2 = p_\rho|_s = \left.\frac{\partial p}{\partial \rho}\right|_s$.

2.1 First-order scheme

Let $I_i = [r_{i-\frac{1}{2}}, r_{i+\frac{1}{2}}]$ be the cell, $\Delta r_i = r_{i+\frac{1}{2}} - r_{i-\frac{1}{2}}$ be the size of the cell and $m_i = \int_{I_i} \rho r dr$ be the mass in the cell I_i, which keeps a constant value during the time marching according to the first equation in (2.1). Then we introduce the cell averaged value in the cell I_i as $\overline{\mathsf{U}}_i = (\overline{\rho}_i, \overline{u}_i, \overline{E}_i)^\top$, in which the averaged values of density, velocity and total energy are defined as follows

$$\overline{\rho}_i = \frac{1}{V_i}\int_{I_i} \rho r dr, \quad \overline{u}_i = \frac{1}{m_i}\int_{I_i} \rho u r dr, \quad \overline{E}_i = \frac{1}{m_i}\int_{I_i} \rho E r dr, \tag{2.2}$$

where $V_i = \int_{I_i} r dr$ denotes the volume of the cell obtained by rotating the cell I_i around the origin of the coordinate (without the 2π factor).

Based on these notations, we can rewrite the system in (2.1) in the following control volume formulation

$$\begin{cases} \overline{\rho}_i = \dfrac{m_i}{V_i}, \\ m_i \dfrac{d}{dt}\overline{u}_i = -(rp)|_{r=r_{i+1/2}} + (rp)|_{r=r_{i-1/2}} + \displaystyle\int_{I_i} p dr, \\ m_i \dfrac{d}{dt}\overline{E}_i = -(rpu)|_{r=r_{i+1/2}} + (rpu)|_{r=r_{i-1/2}}. \end{cases} \tag{2.3}$$

Notice that (2.3) is satisfied by the exact solution of the partial differential equations (PDEs) (2.1) and is not a scheme yet. However, when the point values at the right-hand side in (2.3) are approximated using the cell averages (2.2), it will become a scheme which evolves these cell averages as well as moves the mesh. Moreover, we can get the fully discrete finite volume Lagrangian scheme by using Euler forward time discretization which is as follows,

$$\begin{cases} \overline{\rho}_i^{n+1} = \dfrac{m_i}{V_i^{n+1}}, \\ \overline{u}_i^{n+1} = \overline{u}_i^n - \dfrac{\Delta t^n}{m_i}(r_{i+\frac{1}{2}} p^*_{i+\frac{1}{2}} - r_{i-\frac{1}{2}} p^*_{i-\frac{1}{2}}) + \dfrac{\Delta t^n}{m_i}\Delta r_i P_s, \\ \overline{E}_i^{n+1} = \overline{E}_i^n - \dfrac{\Delta t^n}{m_i}(r_{i+\frac{1}{2}} p^*_{i+\frac{1}{2}} u^*_{i+\frac{1}{2}} - r_{i-\frac{1}{2}} p^*_{i-\frac{1}{2}} u^*_{i-\frac{1}{2}}), \end{cases} \tag{2.4}$$

where P_s is the approximation of the source term, particularly in the first order case it can be taken as $\overline{p}_i^n$. The intercell values $p^*_{i+\frac{1}{2}}$ and $u^*_{i+\frac{1}{2}}$ are the pressure and velocity at the node $r_{i+\frac{1}{2}}$, respectively, obtained from an exact or approximate Riemann solver by giving the left and right states, which are $\overline{\mathsf{U}}_i^n$ and $\overline{\mathsf{U}}_{i+1}^n$ in the first order case. The scheme (2.4) is not complete without the time integration of the trajectory equation, which enables us to advance in the time the grid position, the cell size and volume as

$$\begin{cases} r_{i+\frac{1}{2}}^{n+1} = r_{i+\frac{1}{2}}^n + \Delta t^n u^*_{i+\frac{1}{2}}, \\ \Delta r_i^{n+1} = r_{i+\frac{1}{2}}^{n+1} - r_{i-\frac{1}{2}}^{n+1}, \\ V_i^{n+1} = \dfrac{1}{2}\Delta r_i^{n+1}(r_{i+\frac{1}{2}}^{n+1} + r_{i-\frac{1}{2}}^{n+1}). \end{cases} \tag{2.5}$$

Thus the numerical scheme depends on the choice of the numerical flux, which is generally obtained by exactly or approximately solving the Riemann problem at the cell interface $r_{i+\frac{1}{2}}$ with the given left and right states respectively. In this paper, we will utilize the two-state

Riemann solver proposed in [13, 18]. Specific formulas of this Riemann solver are given in Appendix A, which will be used below. More details can be found in [13, 18].

2.2 First-order positivity-preserving scheme

For the desired property, we define the set of admissible states by

$$G = \left\{ \mathsf{U} = \begin{pmatrix} \rho \\ u \\ E \end{pmatrix},\ \rho > 0,\ e = E - \frac{1}{2}|u|^2 > 0 \text{ and } a^2 = p_\rho|_s > 0 \right\}. \tag{2.6}$$

Lemma 2.1. *The set of admissible states G is a convex set, referring to* [5, 18, 21].

The scheme (2.4) is called positivity-preserving if $\{\overline{\mathsf{U}}_i^n \in G, i = 1, \ldots, N\}$ implies $\{\overline{\mathsf{U}}_i^{n+1} \in G, i = 1, \ldots, N\}$.

By adding and subtracting $\frac{\Delta t^n}{m_i}\Delta r_i^n \overline{p}_i^n$ in the second equation of (2.4), the scheme (2.4) can be rewritten as

$$\begin{aligned} \overline{\mathsf{U}}_i^{n+1} &= \begin{pmatrix} \overline{\rho}_i^{n+1} \\ \overline{u}_i^{n+1} \\ \overline{E}_i^{n+1} \end{pmatrix} = \begin{pmatrix} \frac{m_i}{V_i^{n+1}} \\ \overline{u}_i^n - \frac{\Delta t^n}{m_i}(r_{i+\frac{1}{2}} p^*_{i+\frac{1}{2}} - r_{i-\frac{1}{2}} p^*_{i-\frac{1}{2}}) + \frac{\Delta t^n}{m_i}\Delta r_i^n \overline{p}_i^n + \frac{\Delta t^n}{m_i}\Delta r_i^n (P_s - \overline{p}_i^n) \\ \overline{E}_i^n - \frac{\Delta t^n}{m_i}(r_{i+\frac{1}{2}} p^*_{i+\frac{1}{2}} u^*_{i+\frac{1}{2}} - r_{i-\frac{1}{2}} p^*_{i-\frac{1}{2}} u^*_{i-\frac{1}{2}}) \end{pmatrix} \\ &= \frac{1}{2}\mathsf{H} + \frac{1}{2}\mathsf{W}, \end{aligned} \tag{2.7}$$

where

$$\begin{aligned} \mathsf{H} &= \begin{pmatrix} \frac{m_i}{V_i^{n+1}} \\ \overline{u}_i^n - \frac{2\Delta t^n}{m_i}(r_{i+\frac{1}{2}} p^*_{i+\frac{1}{2}} - r_{i-\frac{1}{2}} p^*_{i-\frac{1}{2}}) + \frac{2\Delta t^n}{m_i}\Delta r_i^n \overline{p}_i^n \\ \overline{E}_i^n - \frac{2\Delta t^n}{m_i}(r_{i+\frac{1}{2}} p^*_{i+\frac{1}{2}} u^*_{i+\frac{1}{2}} - r_{i-\frac{1}{2}} p^*_{i-\frac{1}{2}} u^*_{i-\frac{1}{2}}) \end{pmatrix}, \\ \mathsf{W} &= \begin{pmatrix} \frac{m_i}{V_i^{n+1}} \\ \overline{u}_i^n + \frac{2\Delta t^n}{m_i}\Delta r_i^n (P_s - \overline{p}_i^n) \\ \overline{E}_i^n \end{pmatrix}. \end{aligned} \tag{2.8}$$

It is obvious that $\overline{\mathsf{U}}_i^{n+1}$ is a convex combination of H and W. To ensure that $\overline{\mathsf{U}}_i^{n+1}$ can preserve the positivity property, we could consider the sufficient condition that both H and W are positivity-preserving.

Before that, we would also want to obey the classical CFL condition, which reads as

$$\Delta t^n \leq \lambda \min_i \frac{\Delta r_i^n}{\overline{a}_i^n} = \Delta t_1, \tag{2.9}$$

where $\lambda \leq 1$ is the Courant number (we take $\lambda = 0.5$ in our computation), and $\overline{a}_i^n$ is the sound speed determined by cell averages. Meanwhile, in order to ensure that the cells will not degenerate after the time step Δt^n, we would add another restriction on the time step as follows

$$\Delta t^n \leq \widetilde{\lambda} \min_i \left(\frac{\Delta r_i^n}{(u^*_{i-\frac{1}{2}} - u^*_{i+\frac{1}{2}})^+}, \frac{r^n_{i+\frac{1}{2}}}{(-u^*_{i+\frac{1}{2}})^+} \right) = \Delta t_2, \tag{2.10}$$

where $c^+ = \max(c, 0)$ and $\widetilde{\lambda} < 1/2$ (we take $\widetilde{\lambda} = 0.4$ in our computation). This condition guarantees the size of each cell $\Delta r_i > 0$ and the position $r_{i+\frac{1}{2}} > 0$, then $V_i > 0$, which can ensure the positivity of density based on the first equality in the scheme (2.4).

Motivated by [18, 19], we put an additional constraint on the time step as

$$\Delta t^n \leq \min_i \frac{\sigma V_i^n}{\left| r_{i+\frac{1}{2}} u^*_{i+\frac{1}{2}} - r_{i-\frac{1}{2}} u^*_{i-\frac{1}{2}} \right|} = \min_i \frac{\sigma m_i}{\overline{\rho}_i^n \left| r_{i+\frac{1}{2}} u^*_{i+\frac{1}{2}} - r_{i-\frac{1}{2}} u^*_{i-\frac{1}{2}} \right|} = \Delta t_3, \tag{2.11}$$

where $0 < \sigma < 1$, then we can ensure that the volume changes at most by a factor σ from t^n to t^{n+1} and hope to achieve positive internal energy by determining the factor σ.

Now we focus on finding the required condition to ensure the internal energy $e(\mathsf{H}) = E(\mathsf{H}) - \frac{1}{2}(u(\mathsf{H}))^2 > 0$ in the similar way as that in [18]. Detailed derivation is omitted and we can determine the factor σ in (2.11) as $\sigma \leq \min(1, \frac{1}{2}\frac{\overline{\rho}_i^n \overline{e}_i^n}{|\overline{p}_i^n|})$ and obtain another time step restriction

$$\Delta t^n \leq \min_i \frac{m_i}{r_{i-\frac{1}{2}} \widetilde{z}^+_{i-\frac{1}{2}} + r_{i+\frac{1}{2}} \widetilde{z}^-_{i+\frac{1}{2}}} = \Delta t_4, \tag{2.12}$$

for the scheme (2.4). In particular, for the acoustic solver case, i.e. $\widetilde{z}^+_{i-\frac{1}{2}} = \widetilde{z}^-_{i+\frac{1}{2}} = \overline{\rho}_i^n \overline{a}_i^n$, this condition writes $\Delta t^n \leq \frac{\Delta r_i^n}{2\overline{a}_i^n}$, which can be recovered by the classic CFL condition (2.9) when $\lambda = 0.5$.

As for the sufficient condition for $\mathsf{W} \in G$. Similarly, we only need to solve the quadratic inequality $e(\mathsf{W}) = E(\mathsf{W}) - \frac{1}{2}(u(\mathsf{W}))^2 \geq 0$, which is guaranteed if

$$\Delta t^n \leq \min_i \left(-\frac{m_i \overline{u}_i^n}{2\mu} + \frac{m_i}{2|\mu|} \sqrt{(\overline{u}_i^n)^2 + 2\overline{e}_i^n} \right) = \Delta t_5, \tag{2.13}$$

with $\mu = \Delta r_i^n(P_s - \overline{p}_i^n)$. In particular, when we choose P_s as $\overline{p}_i^n$ for the first order approximation of the source term, the condition (2.13) always holds for any Δt^n.

Theorem 2.2. *For the first order Lagrangian scheme* (2.4) *with the numerical fluxes defined in the two-state Riemann solver and any general positive wavespeeds definition, assuming* $\overline{\mathsf{U}}_i^n \in G$, $\overline{\mathsf{U}}_i^{n+1}$ *is ensured to be in the admissible set* G *under the following time step constraint condition*

$$\Delta t^n \leq \min(\Delta t_1, \Delta t_2, \Delta t_3, \Delta t_4, \Delta t_5), \tag{2.14}$$

where Δt_1 *is the classical CFL condition defined in* (2.9), Δt_2 *is defined by* (2.10), Δt_3 *reads as that in* (2.11) *with* $\sigma \leq \min(1, \frac{1}{2}\frac{\overline{\rho}_i^n \overline{e}_i^n}{|\overline{p}_i^n|})$, Δt_4 *is defined in* (2.12) *and* Δt_5 *is defined in* (2.13) *with* $\mu = \Delta r_i^n(P_s - \overline{p}_i^n)$.

Now, let us make a summary about the first-order positivity-preserving scheme (2.4) and give the algorithm flowchart for it at each time step:

(1) Assuming $\overline{\mathsf{U}}_i \in G$ at the n-th time level, compute the numerical fluxes $p^*_{i+\frac{1}{2}}$ and $u^*_{i+\frac{1}{2}}$ for all i by (A.2).

(2) Compute the time step Δt^n by (2.14).

(3) Update the position of each cell vertex, and obtain the size and volume of each cell by (2.5).

(4) Compute the averaged values $\overline{\mathsf{U}}_i$ at the $(n+1)$-th time level based on the scheme (2.4).

2.3 High-order scheme

Now, we consider a general high-order finite volume Lagrangian scheme which has the same general form as the first order Lagrangian scheme (2.4), where P_s is the approximation with high order accuracy of the source term $\frac{1}{\Delta r_i}\int_{I_i} p dr$. For instance, if we perform a third order scheme, we can compute P_s using the Gauss-Lobatto quadrature rule $P_s = \frac{1}{6}p^+_{i-\frac{1}{2}} + \frac{2}{3}p_i + \frac{1}{6}p^-_{i+\frac{1}{2}}$.

For a high-order accurate spacial discretization, by the information of the corresponding cell-average variables from the cell I_i and its neighboring cells, we apply the techniques of essentially non-oscillatory (ENO) reconstruction and local characteristic decomposition [10] to obtain reconstruction polynomials, through which we can determine the values at the cell interfaces $\{\mathsf{U}^{\mp}_{i\pm\frac{1}{2}}\}$. Then the numerical fluxes $p^*_{i+\frac{1}{2}}$ and $u^*_{i+\frac{1}{2}}$ for all i can be computed by the two-state Riemann solver stated in (A.1)-(A.2).

In this section, we consider the ENO reconstruction by treating the cell averages as integrals on the usual control volumes. This is simply a standard reconstruction which can be made arbitrarily high order accurate by increasing the polynomial degrees and the stencils.

We perform the ENO reconstruction on the conserved variables, namely density, momentum and total energy $(\rho, \rho u, \rho E)^\top$, with a set of polynomials $\{W_i(r) = (\rho_i(r), \mathcal{M}_i(r), \mathcal{E}_i(r))^\top\}$ of degree $k \geq 1$ in the cell I_i for each i, which implies

$$\begin{aligned}
\overline{\rho}_i &= \frac{1}{V_i}\int_{I_i} \rho_i(r) r dr = \frac{m_i}{V_i}, \\
\overline{\mathcal{M}}_i &= \frac{1}{V_i}\int_{I_i} \mathcal{M}_i(r) r dr = \frac{\int_{I_i} \mathcal{M}_i(r) r dr}{m_i} \cdot \frac{m_i}{V_i} = \overline{\rho}_i \cdot \overline{u}_i, \\
\overline{\mathcal{E}}_i &= \frac{1}{V_i}\int_{I_i} \mathcal{E}_i(r) r dr = \frac{\int_{I_i} \mathcal{E}_i(r) r dr}{m_i} \cdot \frac{m_i}{V_i} = \overline{\rho}_i \cdot \overline{E}_i.
\end{aligned} \tag{2.15}$$

If we use polynomials of degree k in the reconstruction process, we obtain a $(k+1)$-th order scheme.

2.4 High-order positivity-preserving schemes

In this section, we focus on how to design the high order scheme (2.4) to be positivity-preserving when applying the ENO reconstruction (2.15).

Before that, let us consider the K-point Legendre Gauss-Lobatto quadrature rule in the interval I_i, which is exact for integrals of polynomials with degree up to $2K-3$, and we denote these quadrature points in I_i as

$$S_i = \{r_{i-\frac{1}{2}} = r_i^1, r_i^2, \ldots, r_i^{K-1}, r_i^K = r_{i+\frac{1}{2}}\}. \tag{2.16}$$

Let ω_α be the quadrature weights such that $\omega_\alpha > 0, \alpha = 1, \ldots, K$, $\omega_1 = \omega_K$, and $\sum_{\alpha=1}^{K} \omega_\alpha = 1$.

Assuming that we perform the ENO reconstruction as in (2.15), we get a polynomial vector $\{W_i(r) = (\rho_i(r), \mathcal{M}_i(r), \mathcal{E}_i(r))^\top\}$ of degree $k \geq 1$. We choose K to be the smallest integer satisfying $2K - 3 \geq k + 1$, then the K-point Legendre Gauss-Lobatto quadrature rule is exact for the integrals involved in the reconstruction (2.15), hence we have

$$\overline{W}_i V_i = \sum_{\alpha=1}^{K} \omega_\alpha W_{\alpha i} r_i^\alpha \Delta r_i = (\omega_1 W^+_{i-\frac{1}{2}} r_{i-\frac{1}{2}} + \widetilde{\omega}_i^* W_i^* + \omega_K W^-_{i+\frac{1}{2}} r_{i+\frac{1}{2}}) \Delta r_i,$$

with

$$\widetilde{\omega}_i^* = \sum_{\alpha=2}^{K-1} \omega_\alpha r_i^\alpha, \quad W_i^* = \frac{1}{\widetilde{\omega}_i^*} \sum_{\alpha=2}^{K-1} \omega_\alpha W_{\alpha i} r_i^\alpha = \frac{1}{\widetilde{\omega}_i^*} \left(\frac{\overline{W}_i V_i}{\Delta r_i} - \omega_1 W^+_{i-\frac{1}{2}} r_{i-\frac{1}{2}} - \omega_K W^-_{i+\frac{1}{2}} r_{i+\frac{1}{2}} \right), \tag{2.17}$$

which implies

$$\begin{aligned} \overline{\rho}_i &= \frac{1}{V_i} \int_{I_i} \rho_i(r) r dr = \frac{1}{V_i} \sum_{\alpha=1}^{K} \omega_\alpha m_{\alpha i}, \\ \overline{u}_i &= \frac{1}{m_i} \int_{I_i} \mathcal{M}_i(r) r dr = \frac{1}{m_i} \sum_{\alpha=1}^{K} \omega_\alpha m_{\alpha i} u_{\alpha i}, \\ \overline{E}_i &= \frac{1}{m_i} \int_{I_i} \mathcal{E}_i(r) r dr = \frac{1}{m_i} \sum_{\alpha=1}^{K} \omega_\alpha m_{\alpha i} E_{\alpha i}, \end{aligned} \tag{2.18}$$

where $m_{\alpha i} = \rho_{\alpha i} r_i^\alpha \Delta r_i^n$ with

$$\rho_{\alpha i} = \rho_i(r_i^\alpha), \quad u_{\alpha i} = \frac{\mathcal{M}_i(r_i^\alpha)}{\rho_i(r_i^\alpha)}, \quad E_{\alpha i} = \frac{\mathcal{E}_i(r_i^\alpha)}{\rho_i(r_i^\alpha)}.$$

Now, let us first introduce the artificial numerical fluxes $\mathfrak{p}_i^*$ and $\mathfrak{u}_i^*$ referring to [18], which are computed from the left and right states $\mathsf{U}^+_{i-\frac{1}{2}}$ and $\mathsf{U}^-_{i+\frac{1}{2}}$. In order to keep accordance with them, we also need to define the artificial local wavespeeds relative to this term, $\widetilde{z}^{\mp,\mathfrak{u}}_{i\pm\frac{1}{2}}$, in the same way as $\widetilde{z}^{\mp}_{i\pm\frac{1}{2}}$. For example, if we take the Dukowicz definition of $\widetilde{z}^{\mp}_{i\pm\frac{1}{2}}$ proposed in [7],

$$\widetilde{z}^{\mp}_{i\pm\frac{1}{2}} = \rho^{\mp}_{i\pm\frac{1}{2}} (a^{\mp}_{i\pm\frac{1}{2}} + \Gamma |u^*_{i\pm\frac{1}{2}} - u^{\mp}_{i\pm\frac{1}{2}}|),$$

the artificial wavespeeds $\widetilde{z}^{\mp,\mathfrak{u}}_{i\pm\frac{1}{2}}$ read as

$$\widetilde{z}^{\mp,\mathfrak{u}}_{i\pm\frac{1}{2}} = \rho^{\mp}_{i\pm\frac{1}{2}} (a^{\mp}_{i\pm\frac{1}{2}} + \Gamma |\mathfrak{u}^*_i - u^{\mp}_{i\pm\frac{1}{2}}|),$$

where the artificial velocity $\mathfrak{u}_i^*$ and artificial pressure $\mathfrak{p}_i^*$ read as

$$\mathfrak{u}_i^* = \frac{\widetilde{z}^{+,\mathfrak{u}}_{i-\frac{1}{2}} u^+_{i-\frac{1}{2}} + \widetilde{z}^{-,\mathfrak{u}}_{i+\frac{1}{2}} u^-_{i+\frac{1}{2}}}{\widetilde{z}^{+,\mathfrak{u}}_{i-\frac{1}{2}} + \widetilde{z}^{-,\mathfrak{u}}_{i+\frac{1}{2}}} - \frac{1}{\widetilde{z}^{+,\mathfrak{u}}_{i-\frac{1}{2}} + \widetilde{z}^{-,\mathfrak{u}}_{i+\frac{1}{2}}}(p^-_{i+\frac{1}{2}} - p^+_{i-\frac{1}{2}}),$$
$$\mathfrak{p}_i^* = \frac{\widetilde{z}^{+,\mathfrak{u}}_{i-\frac{1}{2}} p^-_{i+\frac{1}{2}} + \widetilde{z}^{-,\mathfrak{u}}_{i+\frac{1}{2}} p^+_{i-\frac{1}{2}}}{\widetilde{z}^{+,\mathfrak{u}}_{i-\frac{1}{2}} + \widetilde{z}^{-,\mathfrak{u}}_{i+\frac{1}{2}}} - \frac{\widetilde{z}^{+,\mathfrak{u}}_{i-\frac{1}{2}} \widetilde{z}^{-,\mathfrak{u}}_{i+\frac{1}{2}}}{\widetilde{z}^{+,\mathfrak{u}}_{i-\frac{1}{2}} + \widetilde{z}^{-,\mathfrak{u}}_{i+\frac{1}{2}}}(u^-_{i+\frac{1}{2}} - u^+_{i-\frac{1}{2}}).$$

If we take the acoustic impedance $\widetilde{z}^{\mp}_{i\pm\frac{1}{2}} = \rho^{\mp}_{i\pm\frac{1}{2}} a^{\mp}_{i\pm\frac{1}{2}}$, there will be no difference, i.e. $\widetilde{z}^{\mp,\mathfrak{u}}_{i\pm\frac{1}{2}} = \widetilde{z}^{\mp}_{i\pm\frac{1}{2}}$.

Then, by adding and subtracting $\frac{\Delta t^n}{m_i}\Delta r_i \mathfrak{p}_i^*$ in the second equation in (2.4) and $\frac{\Delta t^n}{m_i}\Delta r_i \mathfrak{p}_i^* \mathfrak{u}_i^*$ in the third equation in (2.4) respectively, the scheme (2.4) becomes

$$\overline{\mathsf{U}}_i^{n+1} = \frac{1}{2}\mathsf{H} + \frac{1}{2}\mathsf{W}, \tag{2.19}$$

where

$$\mathsf{H} = \begin{pmatrix} \dfrac{m_i}{V_i^{n+1}} \\ \overline{u}_i^n - \dfrac{2\Delta t^n}{m_i}(r_{i+\frac{1}{2}} p^*_{i+\frac{1}{2}} - r_{i-\frac{1}{2}} p^*_{i-\frac{1}{2}}) + \dfrac{2\Delta t^n}{m_i}\Delta r_i \mathfrak{p}_i^* \\ \overline{E}_i^n - \dfrac{2\Delta t^n}{m_i}(r_{i+\frac{1}{2}} p^*_{i+\frac{1}{2}} u^*_{i+\frac{1}{2}} - r_{i-\frac{1}{2}} p^*_{i-\frac{1}{2}} u^*_{i-\frac{1}{2}}) + \dfrac{2\Delta t^n}{m_i}\Delta r_i \mathfrak{p}_i^* \mathfrak{u}_i^* \end{pmatrix}, \tag{2.20}$$

and

$$\mathsf{W} = \begin{pmatrix} \dfrac{m_i}{V_i^{n+1}} \\ \overline{u}_i^n + \dfrac{2\Delta t^n}{m_i}\Delta r_i (P_s - \mathfrak{p}_i^*) \\ \overline{E}_i^n - \dfrac{2\Delta t^n}{m_i}\Delta r_i \mathfrak{p}_i^* \mathfrak{u}_i^* \end{pmatrix}. \tag{2.21}$$

We notice that H can be expressed as the following convex combination

$$\mathsf{H} = \frac{m_i^*}{m_i}\widehat{\mathcal{F}}^* + \frac{\omega_1 m_{1i}}{m_i}\widehat{\mathcal{F}}_1 + \frac{\omega_K m_{Ki}}{m_i}\widehat{\mathcal{F}}_K, \tag{2.22}$$

where $m_i^* = \sum_{\alpha=2}^{K-1} \omega_\alpha m_{\alpha i}$, and $\widehat{\mathcal{F}}^* = \frac{1}{m_i^*}\left(\frac{m_i m_i^*}{V_i^{n+1}}, \sum_{\alpha=2}^{K-1} \omega_\alpha m_{\alpha i} u_{\alpha i}, \sum_{\alpha=2}^{K-1} \omega_\alpha m_{\alpha i} E_{\alpha i}\right)^\top$,

$$\hat{\mathcal{F}}_1 = \begin{pmatrix} \dfrac{m_i}{V_i^{n+1}} \\ u^+_{i-\frac{1}{2}} - \dfrac{2\Delta t^n}{\omega_1 m_{1i}}(r_{i-\frac{1}{2}} \mathfrak{p}_i^* - r_{i-\frac{1}{2}} p^*_{i-\frac{1}{2}}) \\ E^+_{i-\frac{1}{2}} - \dfrac{2\Delta t^n}{\omega_1 m_{1i}}(r_{i-\frac{1}{2}} \mathfrak{p}_i^* \mathfrak{u}_i^* - r_{i-\frac{1}{2}} p^*_{i-\frac{1}{2}} u^*_{i-\frac{1}{2}}) \end{pmatrix}, \tag{2.23}$$

$$\hat{\mathcal{F}}_K = \begin{pmatrix} \dfrac{m_i}{V_i^{n+1}} \\ u^-_{i+\frac{1}{2}} - \dfrac{2\Delta t^n}{\omega_K m_{Ki}}(r_{i+\frac{1}{2}} p^*_{i+\frac{1}{2}} - r_{i+\frac{1}{2}}\mathfrak{p}^*_i) \\ E^-_{i+\frac{1}{2}} - \dfrac{2\Delta t^n}{\omega_K m_{Ki}}(r_{i+\frac{1}{2}} p^*_{i+\frac{1}{2}} u^*_{i+\frac{1}{2}} - r_{i+\frac{1}{2}}\mathfrak{p}^*_i \mathfrak{u}^*_i) \end{pmatrix}. \tag{2.24}$$

We can see that H is a convex combination of three different terms in (2.22). Consequently, if these terms belong to the convex admissible set G, then so does H. Among these terms, $\widehat{\mathcal{F}}^*$ only consists of the polynomial solution at the time level n at the interior Gauss-Lobatto quadrature points. To ensure this quantity to be in G, a particular limitation will be designed in the later section.

We notice that $\hat{\mathcal{F}}_1$ and $\hat{\mathcal{F}}_K$ exactly mimic the first order scheme (2.4) but without the source term. Thus we would like to apply the similar analysis as that in the first-order scheme and then obtain $\hat{\mathcal{F}}_1, \hat{\mathcal{F}}_K \in G$ under the following condition

$$\begin{aligned} \Delta t^n \leq & \omega_1 \min_i \left(\frac{\sigma_1 \Delta r_i^n}{\left|\mathfrak{u}^*_i - u^*_{i-\frac{1}{2}}\right|}, \ \frac{\sigma_2 \Delta r_i^n}{\left|u^*_{i+\frac{1}{2}} - \mathfrak{u}^*_i\right|} \right) = \Delta t_3, \\ \Delta t^n \leq & \omega_1 \min_i \left(\frac{\rho^+_{i-\frac{1}{2}} \Delta r_i^n}{\widetilde{z}^{+,\mathfrak{u}}_{i-\frac{1}{2}} + \widetilde{z}^+_{i-\frac{1}{2}}}, \ \frac{\rho^-_{i+\frac{1}{2}} \Delta r_i^n}{\widetilde{z}^-_{i+\frac{1}{2}} + \widetilde{z}^{-,\mathfrak{u}}_{i+\frac{1}{2}}} \right) = \Delta t_4, \end{aligned} \tag{2.25}$$

with $\sigma_1 \leq \min\left(1, \frac{\rho^+_{i-\frac{1}{2}} e^+_{i-\frac{1}{2}}}{2|p^+_{i-\frac{1}{2}}|}\right), \sigma_2 \leq \min\left(1, \frac{\rho^-_{i+\frac{1}{2}} e^-_{i+\frac{1}{2}}}{2|p^-_{i+\frac{1}{2}}|}\right)$.

As for W, the density is obviously positive. We only need to find a sufficient condition to ensure $e(\mathsf{W}) = E(\mathsf{W}) - \frac{1}{2}u^2(\mathsf{W}) > 0$, which is formulated as

$$\Delta t^n \leq \min_i \left(-\frac{m_i \mu}{2\Delta r_i^n (P_s - \mathfrak{p}^*_i)^2} + \frac{m_i}{2\Delta r_i^n (P_s - \mathfrak{p}^*_i)^2} \sqrt{\mu^2 + 2\overline{e}^n_i (P_s - \mathfrak{p}^*_i)^2} \right) = \Delta t_5, \tag{2.26}$$

with $\mu = \mathfrak{p}^*_i \mathfrak{u}^*_i + (P_s - \mathfrak{p}^*_i)\overline{u}^n_i$.

Theorem 2.3. *If the numerical fluxes are determined by the two-state Riemann solver with any general positive wavespeeds definition, assume* $\overline{\mathsf{U}}^n_i \in G$ *and the polynomial solutions* $\mathsf{U}_{\alpha i} \in G, \alpha = 1, \ldots, K$, *then* $\overline{\mathsf{U}}^{n+1}_i$ *in the high order scheme* (2.4) *with the reconstruction in* (2.15) *is also in the admissible set* G *if*

$$\Delta t^n \leq \min(\Delta t_1, \Delta t_2, \Delta t_3, \Delta t_4, \Delta t_5), \tag{2.27}$$

where Δt_1 is the CFL condition in (2.9)*, $\Delta t_2, \Delta t_3, \Delta t_4$ and Δt_5 are defined in* (2.10)*,* (2.25)-(2.26)*.*

2.5 Positivity-preserving limiter

In order to ensure the positivity property for the high order scheme (2.4), we have assumed that the values of reconstruction polynomials at Gauss-Lobatto quadrature points $\mathsf{U}_{\alpha i} \in G, \alpha = 1, \ldots, K$. To ensure this assumption, we need to make use of the particular limiter introduced in [5, 18, 19, 21].

At the time level n, assume the polynomial reconstruction in the cell I_i is the same as that we presented in the previous section 2.4, i.e $W_i(r)$ with degree k. With the assumption $\overline{\mathsf{U}}_i^n \in G$, we modify the reconstruction polynomial $W_i(r)$ with a constant θ_i as follows

$$\widetilde{W}_i(r) = \overline{W}_i + \theta_i(W_i(r) - \overline{W}_i), \tag{2.28}$$

where $\theta_i \in [0, 1]$ is to be determined, such that $\mathsf{U}(\widetilde{W}_i(r)) \in G$ for all r located in the Gauss-Lobatto quadrature points set S_i defined in (2.16). In fact, we only need to require the three points $W^+_{i-\frac{1}{2}}, W^-_{i+\frac{1}{2}}, W^*_i$ to be in G, where $W^*_i = (\rho^*_i, \mathcal{M}^*_i, \mathcal{E}^*_i)^\top$ is defined in (2.17). Referring to [5, 18, 21], the specific implementation can be taken as follows:

First, let us enforce the admissibility of the density. Choose a small number ε such that $\overline{\rho}_i \geq \varepsilon$ for all i. In practice, we usually take $\varepsilon = 10^{-13}$. For each cell I_i, compute

$$\widehat{\rho}^1_i(r) = \overline{\rho}_i + \theta^1_i(\rho_i(r) - \overline{\rho}_i), \quad \theta^1_i = \min\left\{1, \left|\frac{\overline{\rho}_i - \varepsilon}{\overline{\rho}_i - \rho^+_{i-\frac{1}{2}}}\right|, \left|\frac{\overline{\rho}_i - \varepsilon}{\overline{\rho}_i - \rho^*_i}\right|, \left|\frac{\overline{\rho}_i - \varepsilon}{\overline{\rho}_i - \rho^-_{i+\frac{1}{2}}}\right|\right\}. \tag{2.29}$$

Second, enforce the positivity of the internal energy $e = E - \frac{1}{2}|u|^2$ for each cell. Define $\widehat{W}_i(r) = (\widehat{\rho}_i(r), \mathcal{M}_i(r), \mathcal{E}_i(r))^\top$. For each cell I_i, if $\min\left(e(\widehat{W}^+_{i-\frac{1}{2}}), e(\widehat{W}^*_i), e(\widehat{W}^-_{i+\frac{1}{2}})\right) \geq \varepsilon$ set $\theta^2_i = 1$; otherwise,

$$\theta^2_i = \min\left\{\frac{e(\overline{W}_i)}{e(\overline{W}_i) - e(\widehat{W}^+_{i-\frac{1}{2}})}, \frac{e(\overline{W}_i)}{e(\overline{W}_i) - e(\widehat{W}^*_i)}, \frac{e(\overline{W}_i)}{e(\overline{W}_i) - e(\widehat{W}^-_{i+\frac{1}{2}})}\right\}.$$

Then we get the limited polynomial

$$\widetilde{W}_i(r) = \overline{W}_i + \theta^2_i(\widehat{W}_i(r) - \overline{W}_i). \tag{2.30}$$

It is easy to check that the cell average of $\widetilde{W}_i(r)$ over I_i is not changed and is still $\overline{W}_i^n$, and $\widetilde{W}_{i-\frac{1}{2}}^+, \widetilde{W}_{i+\frac{1}{2}}^-, \widetilde{W}_i^* \in G$. Moreover, the particular limiter does not destroy the high order accuracy in smooth regions and more details and proof can be seen in [20].

2.6 High-order time discretization

To get a global high-order scheme, we generally make use of the classic third order SSP Runge-Kutta type method to for time discretization, whose details can be found in many references such as [5, 18].

At each step, the positivity-preserving limiter is performed to modify the polynomial. Notice that the SSP Runge-Kutta schemes are convex combinations of Euler forward time stepping, thus they are conservative, stable and positivity-preserving when the Euler forward time stepping is conservative, stable and positivity-preserving.

3 Two-dimensional case

In this section, we focus on the compressible Euler system in the two-dimensional cylindrical coordinates. Its specific integral form in the Lagrangian framework can be described as follows

$$\begin{cases} \frac{d}{dt}\iint_{\Omega(t)} \rho r dz dr = 0, \\ \frac{d}{dt}\iint_{\Omega(t)} \rho u_z r dz dr = -\int_{\Gamma(t)} p n_z r dl, \\ \frac{d}{dt}\iint_{\Omega(t)} \rho u_r r dz dr = -\int_{\Gamma(t)} p n_r r dl + \iint_{\Omega(t)} p dz dr, \\ \frac{d}{dt}\iint_{\Omega(t)} \rho E r dz dr = -\int_{\Gamma(t)} p \boldsymbol{u}\cdot\boldsymbol{n} r dl, \end{cases} \tag{3.1}$$

where z and r are the axial and radial directions respectively. $\boldsymbol{u} = (u_z, u_r)$ where u_z, u_r are the velocity components in the z and r directions respectively, and $\boldsymbol{n} = (n_z, n_r)$ is the unit outward normal to the boundary $\Gamma(t)$ in the z-r coordinates.

The geometric conservation law (GCL) means that the rate of change of a Lagrangian control volume should be computed consistently with the node motion, which can be formulated as

$$\frac{d}{dt}\iint_{\Omega(t)} dV = \int_{\Gamma(t)} \boldsymbol{u}\cdot\boldsymbol{n} r dl. \tag{3.2}$$

This property should also hold in the fully-discretized scheme.

3.1 Preliminaries

3.1.1 Basic notations

At first, let us make some notations referring to [4, 6]. Ω is the quadrilateral computational cell with the unique index c. The boundary of the cell Ω_c is $\partial\Omega_c$. Each vertex of the grid has its own unique index p and the counterclockwise ordered list of the vertices of Ω_c is denoted by $p(c)$. V_c and A_c denote the volume and the area of the cell Ω_c respectively. There should be a remark that V_c is obtained by rotating this cell around the azimuthal z-axis (without the 2π factor), which can be formulated as $V_c = \iint\limits_{\Omega_c} r dr dz$.

Similar to (2.2), here we also define the cell averages of density, velocity and total energy as follows:

$$\begin{aligned} \overline{\rho}_c &= \frac{1}{V_c}\iint\limits_{\Omega_c} \rho r dz dr, \qquad \overline{u}_c^z = \frac{1}{m_c}\iint\limits_{\Omega_c} \rho u_z r dz dr, \\ \overline{u}_c^r &= \frac{1}{m_c}\iint\limits_{\Omega_c} \rho u_r r dz dr, \quad \overline{E}_c = \frac{1}{m_c}\iint\limits_{\Omega_c} \rho E r dz dr, \end{aligned} \tag{3.3}$$

where $m_c = \iint\limits_{\Omega_c} \rho r dr dz$ is the mass in the cell Ω_c, which keeps a constant during the time marching according to the first equation in (3.1). With these assumptions, we can rewrite the system (3.1) in the following form

$$\begin{cases} \overline{\rho}_c = \dfrac{m_c}{V_c}, \\ m_c \dfrac{d}{dt}\overline{u}_c^z = -\displaystyle\int\limits_{\partial\Omega_c} p n_z r dl, \\ m_c \dfrac{d}{dt}\overline{u}_c^r = -\displaystyle\int\limits_{\partial\Omega_c} p n_r r dl + \iint\limits_{\Omega_c} p dz dr, \\ m_c \dfrac{d}{dt}\overline{E}_c = -\displaystyle\int\limits_{\partial\Omega_c} p \boldsymbol{u}\cdot\boldsymbol{n} r dl. \end{cases} \tag{3.4}$$

We denote the coordinates and velocity of the vertex p as (z_p, r_p) and $\boldsymbol{u}_p = (u_p^z, u_p^r)$ respectively. l_{pp^+} and l_{pp^-} stand for the length of the edges $[p, p^+]$ and $[p^-, p]$, and $\boldsymbol{n}_{pp^+}$ and $\boldsymbol{n}_{pp^-}$ are the corresponding unit outward norms, where p^- and p^+ are the neighboring vertices of the vertex p, see Figure 3.1.

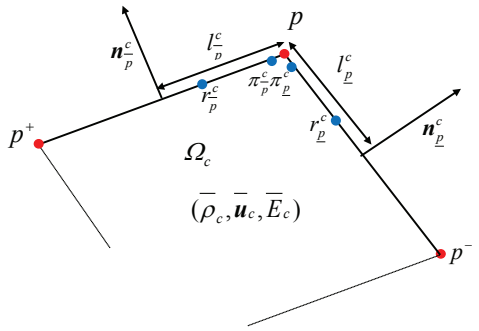

Figure 3.1: Notations of nodes and nodal variables

In order to calculate the discrete gradient operator over the cell Ω_c, we need to denote the two nodal pressures at each vertex p as $\pi_{\underline{p}}^c$ and $\pi_{\overline{p}}^c$, which can be seen in Figure 3.1. These two pressures are related to the two edges sharing the vertex p. With these, we also need to define the half lengths and the unit outward normals of the edges connected to the vertex p in the following way [6]

$$l_{\underline{p}}^c = \frac{1}{2} l_{pp^-}, \qquad l_{\overline{p}}^c = \frac{1}{2} l_{pp^+}, \qquad \boldsymbol{n}_{\underline{p}}^c = \boldsymbol{n}_{pp^-}, \quad \boldsymbol{n}_{\overline{p}}^c = \boldsymbol{n}_{pp^+}. \tag{3.5}$$

Besides, the pseudo-radii $r_{\underline{p}}^c$ and $r_{\overline{p}}^c$ are defined as

$$r_{\underline{p}}^c = \frac{1}{3}(2r_p + r_{p^-}), \quad r_{\overline{p}}^c = \frac{1}{3}(2r_p + r_{p^+}), \tag{3.6}$$

by which the GCL in (3.2) can be rewritten as the following form referring to [6, 12]

$$\frac{d}{dt} V_c(t^n) = \sum_{p \in p(c)} (r_{\underline{p}}^c l_{\underline{p}}^c \boldsymbol{n}_{\underline{p}}^c + r_{\overline{p}}^c l_{\overline{p}}^c \boldsymbol{n}_{\overline{p}}^c) \cdot \boldsymbol{u}_p. \tag{3.7}$$

We will see that the formula is significant for our analysis of positivity preservation in the later section.

Similarly, we denote

$$\begin{aligned} z_{\underline{p}}^c &= \frac{1}{3}(2z_p + z_{p^-}), \qquad z_{\overline{p}}^c = \frac{1}{3}(2z_p + z_{p^+}), \\ \xi_{\underline{p}}^c &= \sqrt{(z_{\underline{p}}^c)^2 + (r_{\underline{p}}^c)^2}, \quad \xi_{\overline{p}}^c = \sqrt{(z_{\overline{p}}^c)^2 + (r_{\overline{p}}^c)^2}. \end{aligned} \tag{3.8}$$

These notations enable us to discretize the right-hand side of (3.4) and get the following semi-discrete form

$$\begin{cases} \overline{\rho}_c = \dfrac{m_c}{V_c}, \\ m_c \dfrac{d}{dt}\overline{u}_c^z = \displaystyle\sum_{p\in p(c)} (r_{\underline{p}}^c l_{\underline{p}}^c \pi_{\underline{p}}^c n_{\underline{p}}^{c,z} + r_{\overline{p}}^c l_{\overline{p}}^c \pi_{\overline{p}}^c n_{\overline{p}}^{c,z}), \\ m_c \dfrac{d}{dt}\overline{u}_c^r = \displaystyle\sum_{p\in p(c)} (r_{\underline{p}}^c l_{\underline{p}}^c \pi_{\underline{p}}^c n_{\underline{p}}^{c,r} + r_{\overline{p}}^c l_{\overline{p}}^c \pi_{\overline{p}}^c n_{\overline{p}}^{c,r}) + \dfrac{\Delta t^n}{m_c} A_c P_s, \\ m_c \dfrac{d}{dt}\overline{E}_c = \displaystyle\sum_{p\in p(c)} (r_{\underline{p}}^c l_{\underline{p}}^c \pi_{\underline{p}}^c \boldsymbol{n}_{\underline{p}}^c + r_{\overline{p}}^c l_{\overline{p}}^c \pi_{\overline{p}}^c \boldsymbol{n}_{\overline{p}}^c) \cdot \boldsymbol{u}_p, \end{cases} \tag{3.9}$$

where $\boldsymbol{n}_{\underline{p}}^c = (n_{\underline{p}}^{c,z}, n_{\underline{p}}^{c,r})$ and $\boldsymbol{n}_{\overline{p}}^c = (n_{\overline{p}}^{c,z}, n_{\overline{p}}^{c,r})$.

3.1.2 Computation of the nodal pressure and velocity

If we denote $\mathsf{U}_{\underline{p}}^c = (\rho_{\underline{p}}^c, \boldsymbol{u}_{\underline{p}}^c, E_{\underline{p}}^c)^\top$, then the nodal pressure $\pi_{\underline{p}}^c$ and $\pi_{\overline{p}}^c$ can be determined in the following way,

$$\begin{aligned} \pi_{\underline{p}}^c &= p_{\underline{p}}^c - \widetilde{z}_{\underline{p}}^c (\boldsymbol{u}_p - \boldsymbol{u}_{\underline{p}}^c) \cdot \boldsymbol{n}_{\underline{p}}^c, \\ \pi_{\overline{p}}^c &= p_{\overline{p}}^c - \widetilde{z}_{\overline{p}}^c (\boldsymbol{u}_p - \boldsymbol{u}_{\overline{p}}^c) \cdot \boldsymbol{n}_{\overline{p}}^c, \end{aligned} \tag{3.10}$$

where $p_{\underline{p}}^c$ and $p_{\overline{p}}^c$ are the pressure values at the vertex p which are computed from $\mathsf{U}_{\underline{p}}^c$ and $\mathsf{U}_{\overline{p}}^c$ respectively. $\widetilde{z}_{\underline{p}}^c$ and $\widetilde{z}_{\overline{p}}^c$ are the approximations of the acoustic impedance. For the sake of the symmetry-preserving property, we limit the choices of $\widetilde{z}_{\underline{p}}^c$ and $\widetilde{z}_{\overline{p}}^c$ to be the Godunov acoustic solver for the two-dimensional case, i.e.

$$\widetilde{z}_{\underline{p}}^c = \rho_{\underline{p}}^c a_{\underline{p}}^c, \quad \widetilde{z}_{\overline{p}}^c = \rho_{\overline{p}}^c a_{\overline{p}}^c, \tag{3.11}$$

which is different from that in the one-dimensional case.

The nodal velocity can be determined uniquely by requiring the scheme to satisfy the conservation of momentum and total energy [12],

$$\boldsymbol{u}_p = M_p^{-1} \sum_{c\in c(p)} \left[r_{\underline{p}}^c l_{\underline{p}}^c [p_{\underline{p}}^c \boldsymbol{n}_{\underline{p}}^c + \widetilde{z}_{\underline{p}}^c (\boldsymbol{n}_{\underline{p}}^c \otimes \boldsymbol{n}_{\underline{p}}^c) \overline{\boldsymbol{u}}_c^n] + r_{\overline{p}}^c l_{\overline{p}}^c [p_{\overline{p}}^c \boldsymbol{n}_{\overline{p}}^c + \widetilde{z}_{\overline{p}}^c (\boldsymbol{n}_{\overline{p}}^c \otimes \boldsymbol{n}_{\overline{p}}^c) \overline{\boldsymbol{u}}_c^n] \right], \tag{3.12}$$

where the matrix M_p reads as

$$M_p = \sum_{c\in c(p)} M_{pc}, \quad M_{pc} = r_{\underline{p}}^c l_{\underline{p}}^c \widetilde{z}_{\underline{p}}^c (\boldsymbol{n}_{\underline{p}}^c \otimes \boldsymbol{n}_{\underline{p}}^c) + r_{\overline{p}}^c l_{\overline{p}}^c \widetilde{z}_{\overline{p}}^c (\boldsymbol{n}_{\overline{p}}^c \otimes \boldsymbol{n}_{\overline{p}}^c) \tag{3.13}$$

with M_{pc} being the projection matrix along the two normals $\boldsymbol{n}_{\underline{p}}^c$ and $\boldsymbol{n}_{\overline{p}}^c$.

3.2 First-order scheme

Based on the notations and assumptions in previous subsections, we can rewrite (3.9) as the following fully discrete finite volume Lagrangian scheme for the PDE system (3.1) in the two-dimensional case

$$\overline{\mathsf{U}}_c^{n+1} = \begin{pmatrix} \overline{\rho}_c^{n+1} \\ \overline{u}_c^{z,n+1} \\ \overline{u}_c^{r,n+1} \\ \overline{E}_c^{n+1} \end{pmatrix} = \begin{pmatrix} \dfrac{m_c}{V_c^{n+1}} \\ \overline{u}_c^{z,n} - \dfrac{\Delta t^n}{m_c} \displaystyle\sum_{p\in p(c)} (r_{\underline{p}}^c l_{\underline{p}}^c \pi_{\underline{p}}^c n_{\underline{p}}^{c,z} + r_{\overline{p}}^c l_{\overline{p}}^c \pi_{\overline{p}}^c n_{\overline{p}}^{c,z}) \\ \overline{u}_c^{r,n} - \dfrac{\Delta t^n}{m_c} \displaystyle\sum_{p\in p(c)} (r_{\underline{p}}^c l_{\underline{p}}^c \pi_{\underline{p}}^c n_{\underline{p}}^{c,r} + r_{\overline{p}}^c l_{\overline{p}}^c \pi_{\overline{p}}^c n_{\overline{p}}^{c,r}) + \dfrac{\Delta t^n}{m_c} A_c P_s \\ \overline{E}_c^n - \dfrac{\Delta t^n}{m_c} \displaystyle\sum_{p\in p(c)} (r_{\underline{p}}^c l_{\underline{p}}^c \pi_{\underline{p}}^c \boldsymbol{n}_{\underline{p}}^c + r_{\overline{p}}^c l_{\overline{p}}^c \pi_{\overline{p}}^c \boldsymbol{n}_{\overline{p}}^c) \cdot \boldsymbol{u}_p \end{pmatrix}. \tag{3.14}$$

Once the nodal velocity $\boldsymbol{u}_p$ at the vertex p has been determined by (3.12), the cell vertex and the area and volume of the cell will be updated as follows [12],

$$\begin{aligned} z_p^{n+1} &= z_p^n + \Delta t^n u_p^z, \quad r_p^{n+1} = r_p^n + \Delta t^n u_p^r, \\ A_c^{n+1} &= \sum_{p\in p(c)} (r_{\underline{p}}^{c,n+1} l_{\underline{p}}^{c,n+1} n_{\underline{p}}^{c,r,n+1} + r_{\overline{p}}^{c,n+1} l_{\overline{p}}^{c,n+1} n_{\overline{p}}^{c,r,n+1}), \\ V_c^{n+1} &= \frac{1}{4} A_c^{n+1} \sum_{p\in p(c)} r_p^{n+1}. \end{aligned} \tag{3.15}$$

3.3 First-order positivity- and symmetry-preserving scheme

In this section, we will discuss how to obtain the significant properties of positivity- and symmetry-preserving for the scheme (3.14).

Before that, let us recall the general CFL condition for the two-dimensional case, which is formulated as

$$\Delta t^n \le \lambda \min_c \frac{l_c^n}{\overline{a}_c^n} = \Delta t_1, \tag{3.16}$$

where we again take the Courant number $\lambda = 0.5$, l_c^n is the length of the shortest edge of the cell Ω_c and $\overline{a}_c^n$ is the sound speed computed by the cell averages. At the same time, to avoid the degeneration of the cells, the time step should also be restricted as follows

$$\Delta t^n \le \widetilde{\lambda} \min_c \left(\frac{2A_c^n}{(b+\widetilde{b}^+)^+}, \min_{p\in p(c)} \frac{r_p^n}{(-u_p^r)^+}, 1 \right) = \Delta t_2, \tag{3.17}$$

where $b = \sum_{p\in p(c)} (r_p u^z_{p^+} + z_{p^+} u^r_p - z_p u^r_{p^+} - r_{p^+} u^z_p)$, $\widetilde{b} = \sum_{p\in p(c)} (u^r_p u^z_{p^+} - u^r_{p^+} u^z_p)$, $b^+ = \max(b, 0)$ and $\widetilde{\lambda} < \frac{1}{2}$. In practice, we again choose it as 0.4.

Now, we start with the preservation of positivity. To achieve that, we put an additional constraint on the time step [19], which can be formulated as follows

$$\Delta t^n \le \min_c \frac{\sigma V_c^n}{\left| \sum_{p\in p(c)} (r^c_{\underline{p}} l^c_{\underline{p}} \boldsymbol{n}^c_{\underline{p}} + r^c_{\overline{p}} l^c_{\overline{p}} \boldsymbol{n}^c_{\overline{p}}) \cdot \boldsymbol{u}_p \right|} = \min_c \frac{\sigma m_c}{\overline{\rho}^n_c \left| \sum_{p\in p(c)} (r^c_{\underline{p}} l^c_{\underline{p}} \boldsymbol{n}^c_{\underline{p}} + r^c_{\overline{p}} l^c_{\overline{p}} \boldsymbol{n}^c_{\overline{p}}) \cdot \boldsymbol{u}_p \right|} = \Delta t_3, \tag{3.18}$$

with the factor $\sigma \in (0, 1)$ to be determined.

Similarly, we define the admissible set G as

$$G = \left\{ \mathsf{U} = \begin{pmatrix} \rho \\ \boldsymbol{u} \\ E \end{pmatrix}, \ \rho > 0, \ e = E - \frac{1}{2}|\boldsymbol{u}|^2 > 0 \text{ and } a^2 = p_\rho|_s > 0 \right\}. \tag{3.19}$$

Making use of the scheme (3.14), we can know that the density will be positive as long as the volume of the cell, V_c, is positive, which can be ensured under the restriction in (3.17) since we update the cell position by (3.15). Therefore, we will pay more attention to the positivity of the internal energy.

By adding and subtracting $\frac{\Delta t^n}{m_c} \sum_{p\in p(c)} (r^c_{\underline{p}} l^c_{\underline{p}} n^{c,z}_{\underline{p}} + r^c_{\overline{p}} l^c_{\overline{p}} n^{c,z}_{\overline{p}}) \overline{p}^n_c$ and $\frac{\Delta t^n}{m_c} \sum_{p\in p(c)} (r^c_{\underline{p}} l^c_{\underline{p}} n^{c,r}_{\underline{p}} + r^c_{\overline{p}} l^c_{\overline{p}} n^{c,r}_{\overline{p}}) \overline{p}^n_c$ in the second and third equations in (3.14) respectively, we can partition the system (3.14) into two parts, that is

$$\overline{\mathsf{U}}^{n+1}_c = \begin{pmatrix} \overline{\rho}^{n+1}_c \\ \overline{u}^{z,n+1}_c \\ \overline{u}^{r,n+1}_c \\ \overline{E}^{n+1}_c \end{pmatrix} = \frac{1}{2}\mathsf{H} + \frac{1}{2}\mathsf{W}, \tag{3.20}$$

where

$$\mathsf{H}=\begin{pmatrix}\dfrac{m_c}{V_c^{n+1}}\\ \overline{u}_c^{z,n}-\dfrac{2\Delta t^n}{m_c}\displaystyle\sum_{p\in p(c)}(r_{\underline{p}}^c l_{\underline{p}}^c \pi_{\underline{p}}^c n_{\underline{p}}^{c,z}+r_{\overline{p}}^c l_{\overline{p}}^c \pi_{\overline{p}}^c n_{\overline{p}}^{c,z})+\dfrac{2\Delta t^n}{m_c}\displaystyle\sum_{p\in p(c)}(r_{\underline{p}}^c l_{\underline{p}}^c n_{\underline{p}}^{c,z}+r_{\overline{p}}^c l_{\overline{p}}^c n_{\overline{p}}^{c,z})\overline{p}_c^n\\ \overline{u}_c^{r,n}-\dfrac{2\Delta t^n}{m_c}\displaystyle\sum_{p\in p(c)}(r_{\underline{p}}^c l_{\underline{p}}^c \pi_{\underline{p}}^c n_{\underline{p}}^{c,r}+r_{\overline{p}}^c l_{\overline{p}}^c \pi_{\overline{p}}^c n_{\overline{p}}^{c,r})+\dfrac{2\Delta t^n}{m_c}\displaystyle\sum_{p\in p(c)}(r_{\underline{p}}^c l_{\underline{p}}^c n_{\underline{p}}^{c,r}+r_{\overline{p}}^c l_{\overline{p}}^c n_{\overline{p}}^{c,r})\overline{p}_c^n\\ \overline{E}_c^n-\dfrac{2\Delta t^n}{m_c}\displaystyle\sum_{p\in p(c)}(r_{\underline{p}}^c l_{\underline{p}}^c \pi_{\underline{p}}^c \boldsymbol{n}_{\underline{p}}^c+r_{\overline{p}}^c l_{\overline{p}}^c \pi_{\overline{p}}^c \boldsymbol{n}_{\overline{p}}^c)\cdot\boldsymbol{u}_p\end{pmatrix}, \tag{3.21}$$

and

$$\mathsf{W}=\begin{pmatrix}\dfrac{m_c}{V_c^{n+1}}\\ \overline{u}_c^{z,n}-\dfrac{2\Delta t^n}{m_c}\displaystyle\sum_{p\in p(c)}(r_{\underline{p}}^c l_{\underline{p}}^c n_{\underline{p}}^{c,z}+r_{\overline{p}}^c l_{\overline{p}}^c n_{\overline{p}}^{c,z})\overline{p}_c^n\\ \overline{u}_c^{r,n}-\dfrac{2\Delta t^n}{m_c}\displaystyle\sum_{p\in p(c)}(r_{\underline{p}}^c l_{\underline{p}}^c n_{\underline{p}}^{c,r}+r_{\overline{p}}^c l_{\overline{p}}^c n_{\overline{p}}^{c,r})\overline{p}_c^n+\dfrac{2\Delta t^n}{m_c}A_cP_s\\ \overline{E}_c^n\end{pmatrix}. \tag{3.22}$$

By this way, we express $\overline{\mathsf{U}}_c^{n+1}$ as a convex combination consisting of H and W. Thus, assuming $\overline{\mathsf{U}}_c^n \in G$, if we are able to prove $\mathsf{H},\ \mathsf{W}\in G$, then we can ensure that $\overline{\mathsf{U}}_c^{n+1}\in G$.

Here we follow a similar way to get the sufficient condition for $\mathsf{H}\in G$ as that in one-dimensional case and in [19], and by solving $e(\mathsf{H})>0$ we get $\sigma\le\min(1,\frac{\overline{\rho}_c^n\overline{e}_c^n}{2|\overline{p}_c^n|})$ for (3.18) and the following time step constraint

$$\Delta t^n\le\min_c\frac{m_c}{\displaystyle\sum_{p\in p(c)}(r_{\underline{p}}^c l_{\underline{p}}^c \widetilde{z}_{\underline{p}}^c+r_{\overline{p}}^c l_{\overline{p}}^c \widetilde{z}_{\overline{p}}^c)}=\Delta t_4. \tag{3.23}$$

The sufficient condition for $\mathsf{W}\in G$ can be described as $e(\mathsf{W})>0$. Recalling that in [12]

$$\begin{aligned}\sum_{p\in p(c)}(r_{\underline{p}}^c l_{\underline{p}}^c n_{\underline{p}}^{c,z}+r_{\overline{p}}^c l_{\overline{p}}^c n_{\overline{p}}^{c,z})=0,\\ \sum_{p\in p(c)}(r_{\underline{p}}^c l_{\underline{p}}^c n_{\underline{p}}^{c,r}+r_{\overline{p}}^c l_{\overline{p}}^c n_{\overline{p}}^{c,r})=A_c,\end{aligned} \tag{3.24}$$

we can write $e(\mathsf{W})$ as

$$e(\mathsf{W})=\overline{e}_c^n-2\left(\frac{\Delta t^n}{m_c}\right)^2(A_cP_s-A_c\overline{p}_c^n)^2-\frac{2\Delta t^n}{m_c}(A_cP_s-A_c\overline{p}_c^n)\overline{u}_c^{r,n}. \tag{3.25}$$

This is a quadratic inequality $e(\mathsf{W}) \geq 0$, which is guaranteed by the following condition

$$\Delta t^n \leq \min_c \left(-\frac{m_c \overline{u}_c^{r,n}}{2\mu} + \frac{m_c}{2|\mu|} \sqrt{(\overline{u}_c^{r,n})^2 + 2\overline{e}_c^n} \right) = \Delta t_5, \tag{3.26}$$

with $\mu = A_c(P_s - \overline{p}_c^n)$.

Theorem 3.1. *Consider the first-order scheme* (3.14) *based on the two-state Riemann solver in* (3.10)-(3.13) *for the acoustic definition of wavespeeds* $\widetilde{z}_{\underline{p}}^c$ *and* $\widetilde{z}_{\overline{p}}^c$ *defined in* (3.11). *Assume* $\overline{\mathsf{U}}_c^n \in G$, *then* $\overline{\mathsf{U}}_c^{n+1}$ *is also in the set* G *under the following time step constraints*

$$\Delta t^n \leq \min\left(\Delta t_1, \Delta t_2, \Delta t_3, \Delta t_4, \Delta t_5\right), \tag{3.27}$$

where Δt_1 *is the classic CFL condition* (3.16), $\Delta t_2, \Delta t_3, \Delta t_4, \Delta t_5$ *are defined in* (3.17), (3.18), (3.23), (3.26) *respectively with* $\sigma \leq \min\left(1, \frac{\overline{\rho}_c^n \overline{e}_c^n}{2|\overline{p}_c^n|}\right)$ *for* Δt_3 *and* $\mu = A_c(P_s - \overline{p}_c^n)$ *for* Δt_5.

Now, let us consider a one-dimensional spherical symmetric problem simulated on an equal-angled polar grid, then we know the cell average $\overline{\mathsf{U}}_c = (\overline{\rho}_c, \overline{\boldsymbol{u}}_c, \overline{E}_c)^\top$ in the cell Ω_c are symmetric, which means $\overline{\rho}_c, \overline{E}_c$ and the component of $\overline{\boldsymbol{u}}_c$ in the radial direction are the same in all the cells with the same radial position, while the component of $\overline{\boldsymbol{u}}_c$ in the angular direction is zero for all the cells. According to [6], for the preservation of symmetry, there is a special requirement on the choice of the approximation P_s for pressure in the source term, which should be determined as

$$P_s = \frac{\xi_{\overline{1}}^c \pi_{\overline{1}}^c + \xi_{\underline{2}}^c \pi_{\underline{2}}^c + \xi_{\overline{3}}^c \pi_{\overline{3}}^c + \xi_{\underline{4}}^c \pi_{\underline{4}}^c}{\xi_{\overline{1}}^c + \xi_{\underline{2}}^c + \xi_{\overline{3}}^c + \xi_{\underline{4}}^c}, \tag{3.28}$$

where $\pi_{\overline{1}}^c, \pi_{\underline{2}}^c, \pi_{\overline{3}}^c$ and $\pi_{\underline{4}}^c$ are the values of pressure related to the two radial edges of the cell Ω_c. $\xi_{\overline{1}}^c, \xi_{\underline{2}}^c, \xi_{\overline{3}}^c$ and $\xi_{\underline{4}}^c$ are defined as (3.8).

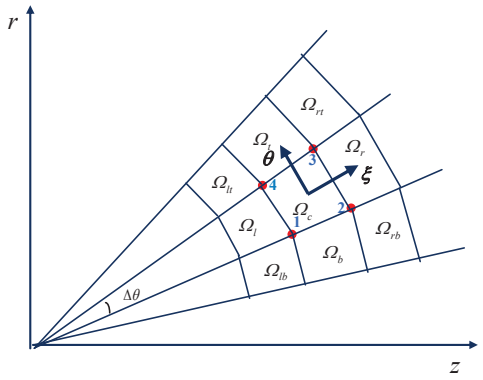

Figure 3.2: The local ξ-θ coordinates for the cell Ω_c.

Theorem 3.2. *The first-order scheme* (3.14) *will keep both positivity and symmetry simultaneously when it is used for a spherical-symmetric problem on an equal-angle-zoned grid, if the time step* Δt^n *satisfies the constraints in Theorem* 3.1 *and* P_s *is taken as* (3.28).

At the end of this section, we make a summary for our first order positivity- and symmetry-preserving Lagrangian scheme (3.14) for two-dimensional cylindrical coordinates and give the following algorithm flowchart.

(1) Assuming $\overline{\mathsf{U}}_c^n \in G$ at the time level n, compute the nodal pressure $\pi_{\underline{p}}^c, \pi_{\overline{p}}^c$ and velocity $\boldsymbol{u}_p$ by (3.10)-(3.13) for all cells.

(2) Compute the pressure in the source term using (3.28).

(3) Compute the time step Δt^n by (3.27).

(4) Update the position of each cell vertex and then compute the area A_c^{n+1} and volume V_c^{n+1} of each cell by (3.15).

(5) Compute the new averaged values $\overline{\mathsf{U}}_c^{n+1}$ by using the scheme (3.14).

3.4 High order scheme

For high order accuracy, the values of $\mathsf{U}_{\underline{p}}^c$ and $\mathsf{U}_{\overline{p}}^c$ at the vertex p in the scheme (3.14) will not be the cell average $\overline{\mathsf{U}}_c$ any more, but can be obtained from the reconstruction polynomials.

Considering a high order scheme, with both positivity and symmetry preservation, we need to reconstruct polynomial functions in each cell Ω_c based on the cell-average information

of the cell Ω_c and its neighbors. Then, the values of $\pi_{\underline{p}}^c, \pi_{\overline{p}}^c$ and $\boldsymbol{u}_p$ can be determined by (3.10)-(3.13).

Here P_s is also determined as (3.28). Besides, if we simulate a spherically symmetric problem, we would hope to keep the symmetry property with the reconstructed polynomials, which puts more restrictions on the reconstruction. We would first need to transform the cell averages of the variables in the neighboring cells which are involved in the reconstruction from the usual (z, r) coordinates to the local polar coordinates (ξ, θ), where ξ stands for the radial direction passing through the center of the edge and the origin, and θ refers to the angular direction, orthogonal to ξ counter-clockwisely. Also, we perform the integral on the area rather than over the usual control volume to get the reconstruction polynomial [6], which can avoid the difficulty caused by different values of r in different cells. This approach of reconstruction will limit the approximation to be at most second order accurate, regardless of reconstruction polynomial degrees. This is however not a restriction in the two-dimensional case as it is known that straight-edge quadrilateral based Lagrangian methods can be at most second order accurate anyway [2].

In this paper, we apply the same technique of reconstruction to get polynomials from the cell averages $\overline{\mathsf{U}}_c^n = (\overline{\rho}_c, \overline{\boldsymbol{u}}_c, \overline{E}_c)^\top$ as that in [6]. Hence we will not give more details about it here.

After we perform the reconstruction on the local ξ-θ coordinates to obtain the polynomials, we transform them into the original z-r coordinates for the calculation of the scheme (3.14). According to [6], after reconstructing along each edge, we get four linear polynomials in the cell Ω_c,

$$\{\mathsf{U}_{m,c}(z,r) = (\rho_{m,c}(z,r), \boldsymbol{u}_{m,c}(z,r), E_{m,c}(z,r))^\top, m = 1\ldots, 4\},$$

which satisfy

$$\iint_{\Omega_c} \mathsf{U}_{m,c}(z,r)dzdr = A_c\overline{\mathsf{U}}_c. \tag{3.29}$$

Here we define the edge sequence $m, m = 1, \ldots, 4$ of the cell Ω_c as those connecting the vertices "1" and "2", "2" and "3","3" and "4","4" and "1" respectively.

3.5 High order positivity- and symmetry-preserving scheme

Assume we have obtained the reconstruction polynomials $\mathsf{U}_{m,c}(z,r)$ along each edge, and by using the relation in (3.29) we can get

$$\overline{\mathsf{U}}_c = \frac{1}{4A_c}\iint_{\Omega_c}\sum_{m=1}^{4}\mathsf{U}_{m,c}(z,r)dzdr. \tag{3.30}$$

If we use a coordinate transformation to convert the cell Ω_c with the general quadrilateral shape in the z-r coordinates to the square $[-\frac{1}{2},\frac{1}{2}]\times[-\frac{1}{2},\frac{1}{2}]$ in the x-y coordinates (see Figure 3.3), we can define the set of Gauss-Lobatto quadrature points for the cell Ω_c to be $S_c=\{(z_\alpha,r_\beta),\alpha=1,\ldots,K,\beta=1,\ldots,K\}$, which are the pre-images under the coordinate transformation of the Gauss-Lobatto quadrature points in the square $[-\frac{1}{2},\frac{1}{2}]\times[-\frac{1}{2},\frac{1}{2}]$. We require the Gauss-Lobatto quadrature rule to be exact for polynomials of degree $2k+1$. This is because a polynomial of degree k in the z-r coordinates becomes a polynomial of degree $2k$ in the x-y coordinates, since the Jacobian of the coordinate transformation is a bilinear function [5].

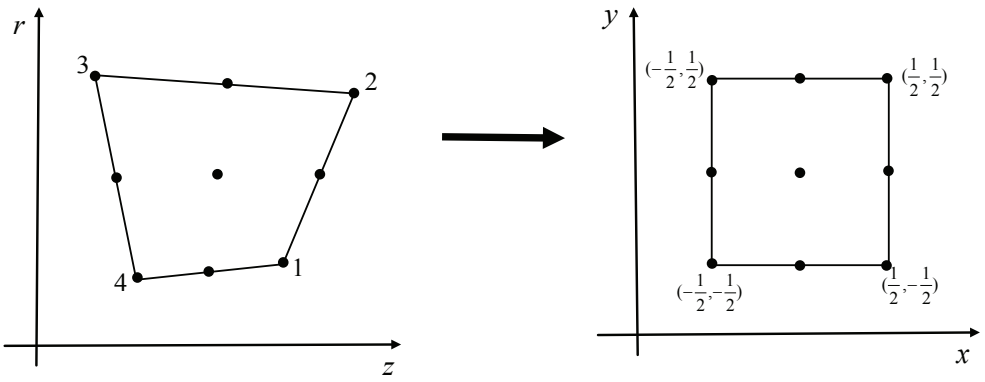

Figure 3.3: The transformation from the z-r coordinates to the x-y coordinates

In fact, since the reconstruction polynomials are linear, we just need to apply the Simpson quadrature rule, in which the quadrature points consist of the cell vertices, the mid-points

of each edge and the cell center, i.e. $K=3$. $\omega_1=\omega_3=\frac{1}{6},\omega_2=\frac{2}{3}$. Based on these, we have

$$\begin{aligned}\overline{\mathsf{U}}_c &= \frac{1}{A_c}\iint_{\Omega_c}\mathsf{U}_{m,c}(z,r)dzdr\\ &= \frac{1}{A_c}\int_{-\frac{1}{2}}^{\frac{1}{2}}\int_{-\frac{1}{2}}^{\frac{1}{2}}\mathsf{U}_{m,c}(g_{m,c}(x,y))\left|\frac{\partial g_{m,c}(x,y)}{\partial(x,y)}\right|dxdy\\ &= \frac{1}{A_c}\sum_{\alpha=1}^{3}\sum_{\beta=1}^{3}\omega_\alpha\omega_\beta\left|\frac{\partial g_{m,c}(x,y)}{\partial(x,y)}\right|_{(x_\alpha,y_\beta)}\mathsf{U}_{m,c}(z_\alpha,r_\beta),\end{aligned}\tag{3.31}$$

where $\mathsf{U}_{m,c}(z_\alpha,r_\beta)$ is the value of $\mathsf{U}_{m,c}(z,r)$ at the corresponding Gauss-Lobatto quadrature points. $\left|\frac{\partial g_{m,c}(x,y)}{\partial(x,y)}\right|$ is the Jacobian for the coordinate transformation [5]. Then if we denote $|J|^{\alpha,\beta}_{m,c}=\left|\frac{\partial g_{m,c}(x,y)}{\partial(x,y)}\right|_{(x_\alpha,y_\beta)}$ and $\mathsf{U}^{m,c}_{\alpha,\beta}=\mathsf{U}_{m,c}(z_\alpha,r_\beta)$, we can rewrite the integral (3.31) by the summation of the values at quadrature points as follows

$$\begin{aligned}\overline{\mathsf{U}}_c &= \frac{1}{4A_c}\iint_{\Omega_c}\sum_{m=1}^{4}\mathsf{U}_{m,c}(z,r)dzdr\\ &= \frac{1}{4}\sum_{m=1}^{4}\omega_*^m\mathsf{U}^*_{m,c}+\sum_{p\in p(c)}(\omega_{\underline{p}}\mathsf{U}^c_{\underline{p}}+\omega_{\overline{p}}\mathsf{U}^c_{\overline{p}}),\end{aligned}\tag{3.32}$$

where

$$\omega_*^1=\frac{1}{A_c}\left(\omega_1\omega_2|J|^{3,2}_{1,c}+\sum_{\alpha=1}^{2}\sum_{\beta=1}^{3}\omega_\alpha\omega_\beta|J|^{\alpha,\beta}_{1,c}\right),\quad \omega_*^2=\frac{1}{A_c}\left(\omega_1\omega_2|J|^{2,3}_{2,c}+\sum_{\alpha=1}^{3}\sum_{\beta=1}^{2}\omega_\alpha\omega_\beta|J|^{\alpha,\beta}_{2,c}\right),$$
$$\omega_*^3=\frac{1}{A_c}\left(\omega_1\omega_2|J|^{1,2}_{3,c}+\sum_{\alpha=2}^{3}\sum_{\beta=1}^{3}\omega_\alpha\omega_\beta|J|^{\alpha,\beta}_{3,c}\right),\quad \omega_*^4=\frac{1}{A_c}\left(\omega_1\omega_2|J|^{2,1}_{4,c}+\sum_{\alpha=1}^{3}\sum_{\beta=2}^{3}\omega_\alpha\omega_\beta|J|^{\alpha,\beta}_{4,c}\right),$$

and

$$\begin{aligned}&\omega_{\underline{1}}=\frac{1}{4A_c}\omega_1^2|J|^{3,1}_{4,c},\quad \omega_{\overline{1}}=\frac{1}{4A_c}\omega_1^2|J|^{3,1}_{1,c},\quad \omega_{\underline{2}}=\frac{1}{4A_c}\omega_1^2|J|^{3,3}_{1,c},\\ &\omega_{\overline{2}}=\frac{1}{4A_c}\omega_1^2|J|^{3,3}_{2,c},\quad \omega_{\underline{3}}=\frac{1}{4A_c}\omega_1^2|J|^{1,3}_{2,c},\quad \omega_{\overline{3}}=\frac{1}{4A_c}\omega_1^2|J|^{1,3}_{3,c},\\ &\omega_{\underline{4}}=\frac{1}{4A_c}\omega_1^2|J|^{1,1}_{3,c},\quad \omega_{\overline{4}}=\frac{1}{4A_c}\omega_1^2|J|^{1,1}_{4,c}.\end{aligned}$$

In fact, we do not need to know the values at the corresponding quadrature points except the nodes at the cell edges according to the Remarks 3.3 and 3.4 in [5], that is to say, we can directly express it as

$$\begin{aligned}&\mathsf{U}^*_{1,c}=\frac{1}{\omega_*^1}\left(A_c\overline{\mathsf{U}}^n_c-4\omega_{\overline{1}}\mathsf{U}^c_{\overline{1}}-4\omega_{\underline{2}}\mathsf{U}^c_{\underline{2}}\right),\quad \mathsf{U}^*_{2,c}=\frac{1}{\omega_*^2}\left(A_c\overline{\mathsf{U}}^n_c-4\omega_{\overline{2}}\mathsf{U}^c_{\overline{2}}-4\omega_{\underline{3}}\mathsf{U}^c_{\underline{3}}\right),\\ &\mathsf{U}^*_{3,c}=\frac{1}{\omega_*^3}\left(A_c\overline{\mathsf{U}}^n_c-4\omega_{\overline{3}}\mathsf{U}^c_{\overline{3}}-4\omega_{\underline{4}}\mathsf{U}^c_{\underline{4}}\right),\quad \mathsf{U}^*_{4,c}=\frac{1}{\omega_*^4}\left(A_c\overline{\mathsf{U}}^n_c-4\omega_{\overline{4}}\mathsf{U}^c_{\overline{4}}-4\omega_{\underline{1}}\mathsf{U}^c_{\underline{1}}\right),\end{aligned}\tag{3.33}$$

which is quite useful when implementing the positivity-preserving limiter.

Therefore, the scheme (3.14) in the high-order case can be rewritten as

$$\overline{\mathsf{U}}_c^{n+1} = \omega^* \mathsf{U}_c^* + \sum_{p\in p(c)} (\omega_{\underline{p}} \hat{\mathcal{F}}_{\underline{p}} + \omega_{\overline{p}} \hat{\mathcal{F}}_{\overline{p}}), \tag{3.34}$$

where $\mathsf{U}_c^* = \frac{1}{4\omega^*} \sum_{m=1}^{4} \omega_*^m \mathsf{U}_{m,c}^*$ but the first component reads as $\frac{m_c}{\omega V_c^{n+1}}$ with $\omega^* = \frac{1}{4} \sum_{m=1}^{4} \omega_*^m$, $\omega = \omega^* + \sum_{p\in p(c)} (\omega_{\underline{p}} + \omega_{\overline{p}})$,

$$\hat{\mathcal{F}}_{\underline{p}} = \begin{pmatrix} \dfrac{m_c}{\omega V_c^{n+1}} \\ u_{\underline{p}}^{c,z} - \dfrac{\Delta t^n}{\omega_{\underline{p}} m_c} r_{\underline{p}}^c l_{\underline{p}}^c \pi_{\underline{p}}^c n_{\underline{p}}^{c,z} \\ u_{\underline{p}}^{c,r} - \dfrac{\Delta t^n}{\omega_{\underline{p}} m_c} r_{\underline{p}}^c l_{\underline{p}}^c \pi_{\underline{p}}^c n_{\underline{p}}^{c,r} + \dfrac{\Delta t^n}{\omega_{\underline{p}} m_c} (\dfrac{1}{8} A_c) P_s \\ E_{\underline{p}}^c - \dfrac{\Delta t^n}{\omega_{\underline{p}} m_c} r_{\underline{p}}^c l_{\underline{p}}^c \pi_{\underline{p}}^c \boldsymbol{n}_{\underline{p}}^c \cdot \boldsymbol{u}_p \end{pmatrix}, \tag{3.35}$$

and

$$\hat{\mathcal{F}}_{\overline{p}} = \begin{pmatrix} \dfrac{m_c}{\omega V_c^{n+1}} \\ u_{\overline{p}}^{c,z} - \dfrac{\Delta t^n}{\omega_{\overline{p}} m_c} r_{\overline{p}}^c l_{\overline{p}}^c \pi_{\overline{p}}^c n_{\overline{p}}^{c,z} \\ u_{\overline{p}}^{c,r} - \dfrac{\Delta t^n}{\omega_{\overline{p}} m_c} r_{\overline{p}}^c l_{\overline{p}}^c \pi_{\overline{p}}^c n_{\overline{p}}^{c,r} + \dfrac{\Delta t^n}{\omega_{\overline{p}} m_c} (\dfrac{1}{8} A_c) P_s \\ E_{\overline{p}}^c - \dfrac{\Delta t^n}{\omega_{\overline{p}} m_c} r_{\overline{p}}^c l_{\overline{p}}^c \pi_{\overline{p}}^c \boldsymbol{n}_{\overline{p}}^c \cdot \boldsymbol{u}_p \end{pmatrix}. \tag{3.36}$$

Obviously, $\overline{\mathsf{U}}_c^{n+1}$ is a convex combination consisting of U_c^* and $\hat{\mathcal{F}}_{\underline{p}}, \hat{\mathcal{F}}_{\overline{p}}$, hence we only need to ensure U_c^* and $\forall p \in p(c), \hat{\mathcal{F}}_{\underline{p}}, \hat{\mathcal{F}}_{\overline{p}}$ are in the admissible set G. For each $\hat{\mathcal{F}}_{\underline{p}}$, we hope to apply exactly the same techniques as those presented in the first order case to make sure $\hat{\mathcal{F}}_{\underline{p}} \in G$ [19], similarly for $\hat{\mathcal{F}}_{\overline{p}} \in G, \forall p \in p(c)$.

Let us define all the corner nodes for each cell as a set $Q_c = \{\underline{1}, \overline{1}, \underline{2}, \overline{2}, \underline{3}, \overline{3}, \underline{4}, \overline{4}\}$ and assume the following formula always holds

$$\sum_{q\in Q_c} r_q^c l_q^c \pi_q^{c,a} \boldsymbol{n}_q^c = \boldsymbol{0}, \tag{3.37}$$

where $\pi_q^{c,a}$ stands for some artificial pressure and its corresponding artificial velocity is $\mathbf{u}_c$ and $\pi_q^{c,a}, \mathbf{u}_c$ are to be determined later.

By adding the artificial term (3.37) in (3.14), $\hat{\mathcal{F}}_{\underline{p}}$ is changed into

$$\hat{\mathcal{F}}_{\underline{p}} = \begin{pmatrix} \dfrac{m_c}{\omega V_c^{n+1}} \\ u_{\underline{p}}^{c,z} - \dfrac{\Delta t^n}{\omega_{\underline{p}} m_c}(r_{\underline{p}}^c l_{\underline{p}}^c \pi_{\underline{p}}^c n_{\underline{p}}^{c,z} - r_{\underline{p}}^c l_{\underline{p}}^c \pi_{\underline{p}}^{c,a} n_{\underline{p}}^{c,z}) \\ u_{\underline{p}}^{c,r} - \dfrac{\Delta t^n}{\omega_{\underline{p}} m_c}(r_{\underline{p}}^c l_{\underline{p}}^c \pi_{\underline{p}}^c n_{\underline{p}}^{c,r} - r_{\underline{p}}^c l_{\underline{p}}^c \pi_{\underline{p}}^{c,a} n_{\underline{p}}^{c,r}) + \dfrac{\Delta t^n}{\omega_{\underline{p}} m_c}(\dfrac{1}{8} A_c) P_s c \\ E_{\underline{p}}^c - \dfrac{\Delta t^n}{\omega_{\underline{p}} m_c}(r_{\underline{p}}^c l_{\underline{p}}^c \pi_{\underline{p}}^c \boldsymbol{n}_{\underline{p}}^c \cdot \boldsymbol{u}_{\underline{p}} - r_{\underline{p}}^c l_{\underline{p}}^c \pi_{\underline{p}}^{c,a} \boldsymbol{n}_{\underline{p}}^c \cdot \mathbf{u}_c) \end{pmatrix}. \tag{3.38}$$

Lemma 3.3. *For all p, $\hat{\mathcal{F}}_{\underline{p}}$ exactly mimics the first order scheme defined in* (3.14)*, so does $\hat{\mathcal{F}}_{\overline{p}}$.*

The proof of this lemma is given in the Appendix B, in which we also show how to define and determine the artificial pressure $\pi_q^{c,a}$ and its corresponding artificial velocity $\mathbf{u}_c$ in (3.37)-(3.38). Therefore, by using the same analysis as that in the first order case, we have the following conclusion.

Theorem 3.4. *Consider the Lagrangian scheme* (3.14) *based on the two-state Riemann solver defined in* (3.10)-(3.13) *with the acoustic definition of $\widetilde{z}_{\underline{p}}^c$ and $\widetilde{z}_{\overline{p}}^c$ defined in* (3.11)*. Assume $\overline{\mathsf{U}}_c^n \in G$ and $\mathsf{U}_{\alpha,\beta}^{m,c} \in G$ for all $m = 1, 4, \alpha, \beta = 1, 3$, then $\overline{\mathsf{U}}_c^{n+1} \in G$ under the following time step constraint*

$$\Delta t^n \leq \min\left(\Delta t_1, \Delta t_2, \Delta t_3, \Delta t_4, \Delta t_5, \Delta t_6\right), \tag{3.39}$$

where Δt_1 is the CFL condition (3.16)*, Δt_2 is defined in* (3.17) *and*

$$\Delta t_3 = \min_{p,c}\left(\frac{2\omega_{\underline{p}} m_c}{\sum\limits_{q\in Q_c} r_q^c l_q^c \widetilde{z}_{\underline{p}}^q}, \ \frac{2\sigma_{\underline{p}}\omega_{\underline{p}} m_c}{\rho_{\underline{p}}^c \left|(\boldsymbol{u}_p - \mathbf{u}_c)\cdot r_{\underline{p}}^c l_{\underline{p}}^c \boldsymbol{n}_{\underline{p}}^c\right|}\right),$$

$$\Delta t_4 = \min_{p,c}\left(\frac{2\omega_{\overline{p}} m_c}{\sum\limits_{q\in Q_c} r_q^c l_q^c \widetilde{z}_{\overline{p}}^q}, \ \frac{2\sigma_{\overline{p}}\omega_{\overline{p}} m_c}{\rho_{\overline{p}}^c \left|(\boldsymbol{u}_p - \mathbf{u}_c)\cdot r_{\overline{p}}^c l_{\overline{p}}^c \boldsymbol{n}_{\overline{p}}^c\right|}\right),$$

with $\sigma_{\underline{p}} \le \min\left(1, \frac{\rho^c_{\underline{p}} e^c_{\underline{p}}}{2|p^c_{\underline{p}}|}\right), \sigma_{\overline{p}} \le \min\left(1, \frac{\rho^c_{\overline{p}} e^c_{\overline{p}}}{2|p^c_{\overline{p}}|}\right)$, *and*

$$\Delta t_5 = \min_{p,c}\left(-\frac{\omega_{\underline{p}} m_c u^{c,r}_{\underline{p}}}{2\mu_1} + \frac{\omega_{\underline{p}} m_c}{2|\mu_1|}\sqrt{(u^{c,r}_{\underline{p}})^2 + 2e^c_{\underline{p}}}\right),$$
$$\Delta t_6 = \min_{p,c}\left(-\frac{\omega_{\overline{p}} m_c u^{c,r}_{\overline{p}}}{2\mu_2} + \frac{\omega_{\overline{p}} m_c}{2|\mu_2|}\sqrt{(u^{c,r}_{\overline{p}})^2 + 2e^c_{\overline{p}}}\right)$$

where

$$\mu_1 = \frac{1}{8}A_c P_s - A_c \pi^c_{\underline{p}}, \qquad \mu_2 = \frac{1}{8}A_c P_s - A_c \pi^c_{\overline{p}}.$$

3.6 Positivity-preserving limiter

To achieve the preservation of symmetry, we need to perform the polynomial reconstruction and positivity-preserving limitation along each edge and in the local ξ-θ coordinates for each cell Ω_c as that we presented before, that is to say, we first need to transform the polynomials in the z-r coordinates $\mathsf{U}_{m,c}(z,r) = (\rho_{m,c}(z,r), \boldsymbol{u}_{m,c}(z,r), E_{m,c}(z,r))^\top$ into the polynomials defined in the ξ-θ coordinates $\mathsf{U}_{m,c}(\xi,\theta) = (\rho_{m,c}(\xi,\theta), \boldsymbol{u}_{m,c}(\xi,\theta), E_{m,c}(\xi,\theta))^\top$.

Under the assumption $\overline{\mathsf{U}}^n_c \in G$, we would like to modify the polynomial reconstruction $\mathsf{U}_{m,c}(\xi,\theta)$ with a constant θ_c into another polynomial $\widetilde{\mathsf{U}}_{m,c}(\xi,\theta)$ such that the values of $\widetilde{\mathsf{U}}_{m,c}(\xi,\theta)$ at its corresponding Gauss-Lobatto quadrature points can be set in G. The implementation is similar to that for the high-order scheme in the one-dimensional case, which can be described as the following modification on the reconstruction polynomial

$$\widetilde{\mathsf{U}}_{m,c}(\xi,\theta) = \overline{\mathsf{U}}_c + \theta_c(\mathsf{U}_{m,c}(\xi,\theta) - \overline{\mathsf{U}}_c), \tag{3.40}$$

where $\theta_c \in [0,1]$ is to be determined, such that $\widetilde{\mathsf{U}}_{m,c}(\xi,\theta) \in G$ for all $(\xi,\theta) \in S_c$.

In fact, we do not need to modify the values at all Gauss-Lobatto quadrature points, we only need to modify the values of $\mathsf{U}_{m,c}(\xi,\theta)$ at the two nodes of its corresponding edge and $\mathsf{U}^*_{m,c}$ defined in (3.33), which represents a lumped contribution from all other Gauss-Lobatto quadrature points.

First, let us enforce the admissibility of the density. Choose a small number ε such that $\overline{\rho}_c \ge \varepsilon$ for all c. In practice, we usually take $\varepsilon = 10^{-13}$. For the each edge of each cell Ω_c,

compute

$$\widehat{\rho}_{m,c}(\xi,\theta)=\overline{\rho}_c+\theta^1_{m,c}(\rho_{m,c}(\xi,\theta)-\overline{\rho}_c),\quad \theta^1_{m,c}=\min\left\{1,\left|\frac{\overline{\rho}_c-\varepsilon}{\overline{\rho}_c-\rho^c_{\widetilde{m}}}\right|,\left|\frac{\overline{\rho}_c-\varepsilon}{\overline{\rho}_c-\rho^c_{\underline{\widetilde{m}}}}\right|,\left|\frac{\overline{\rho}_c-\varepsilon}{\overline{\rho}_c-\rho^*_{m,c}}\right|\right\}, \tag{3.41}$$

with $m=1,2,3,4$ and $\widetilde{m}=1+\bar{m}$ where $\bar{m}=m \pmod 4$.

Second, enforce the positivity of the internal energy e for the cells. Define $\widehat{\mathsf{U}}_{m,c}(\xi,\theta)=(\widehat{\rho}_{m,c}(\xi,\theta),\boldsymbol{u}_{m,c}(\xi,\theta),E_{m,c}(\xi,\theta))^\top$. For the each edge of each cell Ω_c,

$$\theta^2_{m,c}=\min\left\{1,\frac{e(\overline{\mathsf{U}}_c)}{e(\overline{\mathsf{U}}_c)-e(\widehat{\mathsf{U}}^c_{\widetilde{m}})},\ \frac{e(\overline{\mathsf{U}}_c)}{e(\overline{\mathsf{U}}_c)-e(\widehat{\mathsf{U}}^c_{\underline{\widetilde{m}}})},\ \frac{e(\overline{\mathsf{U}}_c)}{e(\overline{\mathsf{U}}_c)-e(\widehat{\mathsf{U}}^*_{m,c})}\right\}.$$

Then we get the following limited polynomial relative to each edge

$$\widetilde{\mathsf{U}}_{m,c}(\xi,\theta)=\overline{\mathsf{U}}_c+\theta^2_{m,c}(\widehat{\mathsf{U}}_{m,c}(\xi,\theta)-\overline{\mathsf{U}}_c). \tag{3.42}$$

After getting the limitation factors $\theta^2_{m,c}$ for $m=1,\ldots,4$, we can get the modified values at two node points along each edge of the cell Ω_c. Then we need to transform back into the z-r coordinates to update the time marching. Performing the limiter in the local ξ-θ coordinates can ensure that the values at the Gauss-Lobatto points with the same radial position and different angular position are the same, thus the property of symmetry can be maintained.

Besides, it is easy to check that the cell average of $\widetilde{\mathsf{U}}_{m,c}(\xi,\theta)$ over Ω_c is not changed and is still $\overline{\mathsf{U}}^n_c$, and $\widetilde{\mathsf{U}}_{m,c}(\xi_\alpha,\theta_\beta)\in G$ for all relevant α,β (including the lumped ones). Moreover, the particular limiter does not destroy the high order accuracy in smooth regions and can keep symmetry.

3.7 High order time discretization

To obtain a Lagrangian scheme with uniformly second order accuracy both in time and space, the time march stepping can be implemented by a second order strong stability preserving (SSP) Runge-Kutta type method, which is detailed in [6].

At each step, the reconstruction polynomials of each cell can be obtained based on the information from itself and its neighbors. Then the limiter operation is performed to modify the polynomial.

4 Numerical examples

In this section, we choose several challenging numerical examples in one- and two-dimensional cylindrical coordinates to show the performance of our first order and high order positivity-preserving and symmetry-preserving Lagrangian schemes. The examples are performed on the ideal gas with $\gamma = 5/3$ unless otherwise stated. The Godunov acoustic solver is used for all numerical tests, i.e. $\widetilde{z} = \rho a$. All these examples encounter the problem of negative internal energy if the usual high order Lagrangian scheme without the positivity-preserving limiter is used.

In order to use larger time steps to improve efficiency as much as possible, we do not restrict the time step as strictly as presented in previous theorems in our actual code. Instead, we just take the time step Δt^n as the minimum of the classical CFL condition and the condition for avoiding degeneration of cells, defined by (2.9)-(2.10) and (3.16)-(3.17) relative to the one- and two-dimensional cases respectively, to march to the time level $n+1$. If the internal energy obtained is positive, we will continue to the next time step; otherwise, we will come back to the previous time level n, and take a smaller time step such as $\frac{1}{2}\Delta t^n$, and proceed as before. The theorems in the previous sections ensure that we only need to come back a finite number of times before we will obtain a positive internal energy. In fact, in our following numerical tests, the coming-back case happens only seldomly.

4.1 One-dimensional tests

Example 1. Accuracy test.

We first test the accuracy of our schemes on a free-expansion problem. The initial

condition is taken as

$$\rho = 1, \quad u = 0, \quad p = 1 - r^4, \quad r \in [0, 1].$$

Free boundary condition is applied on the outer boundary. The errors and accuracy of the scheme at $t = 1$ are listed in Tables 4.1-4.2 which are measured on the interval $[r_{\frac{1}{10}N}, r_{\frac{9}{10}N}]$, where N is the total number of cells, to remove the influence from the boundary. The percentage of the cells (averaged in space and time) in which the positivity-preserving limiter has been performed is also listed in Table 4.2. We take the result of the third order positivity-preserving Lagrangian scheme with 10,000 cells as our reference solution when computing the errors. From these tables, we can clearly see that the first order and third order positivity-preserving schemes with the positivity-preserving limiter have achieved the expected order of accuracy in both L_1 and L_∞ norms for all the evolved conserved variables.

Table 4.1: Errors of the first order scheme in 1D cylindrical coordinates using N initially uniform cells

N	Norm	Density	order	Momentum	order	Energy	order
50	L_1	0.44E-2		0.45E-2		0.56E-2	
	L_∞	0.15E-1		0.85E-2		0.18E-1	
100	L_1	0.23E-2	0.93	0.22E-2	0.97	0.29E-2	0.93
	L_∞	0.78E-2	1.00	0.46E-2	0.86	0.92E-2	0.98
200	L_1	0.11E-2	0.96	0.11E-2	1.00	0.15E-2	0.96
	L_∞	0.39E-2	1.01	0.23E-2	1.01	0.46E-2	1.00
400	L_1	0.61E-3	0.96	0.56E-3	1.01	0.77E-3	0.98
	L_∞	0.19E-2	1.00	0.11E-2	1.08	0.23E-2	0.99
800	L_1	0.32E-3	0.93	0.27E-3	1.02	0.39E-3	0.99
	L_∞	0.97E-3	1.00	0.52E-3	1.05	0.11E-2	0.99

Table 4.2: Errors of the third order scheme with positivity-preserving limiter in 1D cylindrical coordinates using N initially uniform cells

N	Norm	Density	order	Momentum	order	Energy	order	limited cells(%)
50	L_1	0.26E-5		0.28E-5		0.28E-5		0.41
	L_∞	0.72E-5		0.58E-5		0.57E-5		
100	L_1	0.34E-6	2.96	0.35E-6	2.98	0.36E-6	2.93	0.22
	L_∞	0.83E-6	3.10	0.70E-6	3.06	0.82E-6	2.79	
200	L_1	0.34E-7	3.33	0.45E-7	2.98	0.44E-7	3.04	0.16
	L_∞	0.91E-7	3.19	0.80E-7	3.11	0.11E-6	2.85	
400	L_1	0.36E-8	3.22	0.58E-8	2.95	0.53E-8	3.05	0.08
	L_∞	0.12E-7	2.91	0.10E-7	3.01	0.14E-7	2.94	
800	L_1	0.40E-9	3.16	0.78E-9	2.94	0.68E-9	3.02	0.05
	L_∞	0.15E-8	2.96	0.13E-8	2.96	0.19E-8	3.00	

Example 2. Sedov blast wave in a cylindrical coordinate [17].

The initial computational domain is $[0, 1.125]$. The initial condition is

$$\rho = 1, \quad u = 0,$$

The specific internal energy e is 0 except in the cells connected to the origin where they share a total value of 0.244816. In the practical simulation, as we cannot simulate vacuum, e is usually set to be a small positive value such as 10^{-6}. Here we take e to be a smaller positive value, that is 10^{-14} which is demonstrated to bring much more challenge to the scheme. The ideal gas is used with $\gamma = 1.4$. Reflective boundary condition is applied on the outer boundary. The analytical solution is a shock with a peak density of 6 at $r = 1$ and at time $t = 1$. The numerical results with our first and third order schemes using 20 cells at $t = 1$ are shown in Figure 4.1 and convergence plots can be seen in Figure 4.2. We can see the position of the shock has been captured very accurately. Although the internal energy and pressure are quite small, they can always be kept positive.

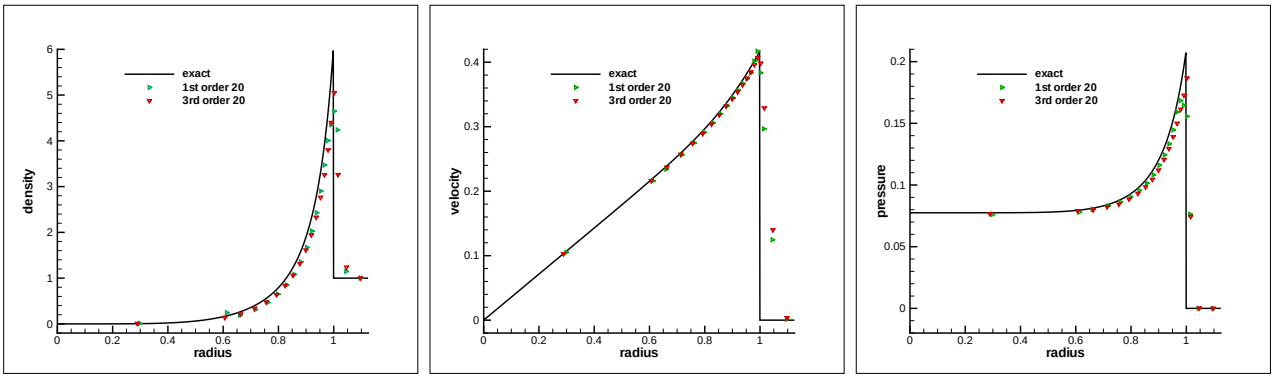

Figure 4.1: The results of the Sedov problem with 20 cells at $t = 1$.

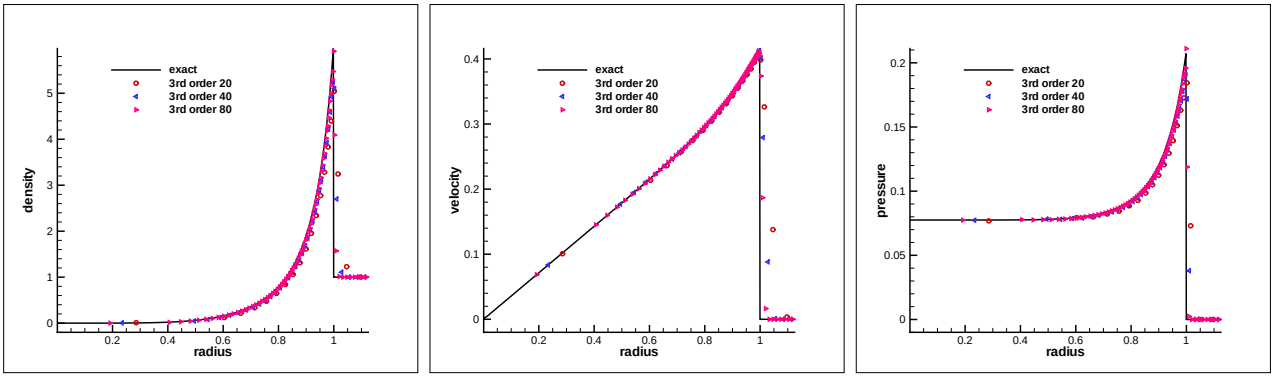

Figure 4.2: The convergence results of the Sedov problem on the meshes with refinement at $t = 1$.

Example 3. The Noh problem in a cylindrical coordinate system [15].

The Noh problem is a classic test problem which is widely used to validate the performance of Lagrangian schemes on strong discontinuities. The initial computational domain is [0,1]. The initial density is 1, the initial pressure is 0, and the initial velocity is directed toward the origin with magnitude 1. The analytic solution is a shock generated by bringing the cold gas to rest at the origin. The density behind the shock is 16, and the shock speed is 1/3. But in practical numerical simulation, we can not take the pressure to be zero. In the literature, the pressure is usually chosen as large as 10^{-5}. However, in this test, to verify the performance of the positivity-preserving property in our scheme, we choose the initial pressure as small as 10^{-13}, which brings significant challenge to the scheme. In fact, the third order Lagrangian scheme fails to compute it without the positivity-preserving limiter,

even with very small time steps. Figures 4.3-4.4 show the results of our first order and third order schemes on the different grids at $t = 0.6$. We can observe that density and pressure are positive and the shock is captured very well, which demonstrates the good performance of our scheme when the pressure and internal energy tend to zero.

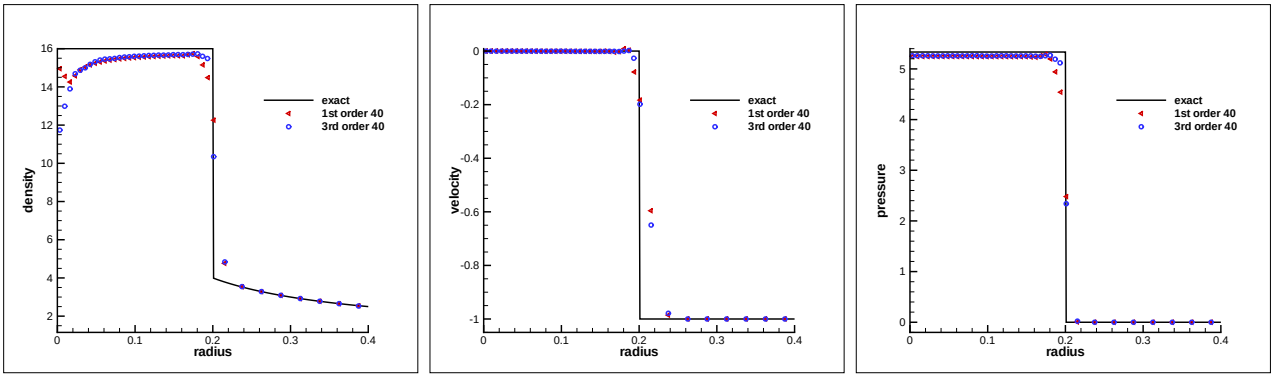

Figure 4.3: The results of the Noh problem with 40 cells at $t = 0.6$.

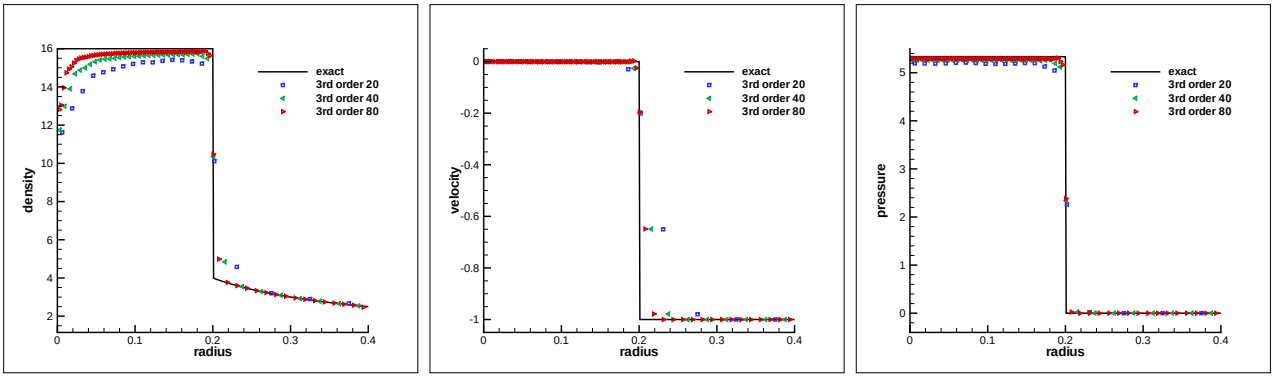

Figure 4.4: The convergence results of the Noh problem with different meshes at $t = 0.6$.

4.2 Two-dimensional tests

In this subsection, we perform numerical experiments in two-dimensional cylindrical coordinates. Purely Lagrangian computation, the initially equal-angled polar grid and the second order scheme (3.14) with (3.10)-(3.13) is used in the following tests unless otherwise stated. Reflective boundary conditions are applied to the z and r axes in all the tests. $\xi = \sqrt{z^2 + r^2}$ is the radial coordinate. u_ξ and u_θ represent the values of velocity in the radial and angular directions in the cell's local polar coordinates.

Example 1. We test the accuracy of the scheme (3.14) on a free expansion problem. The initial computational domain is $[0,1] \times [0,\pi/2]$ defined in the polar coordinates. At $t = 0$, we have

$$\rho = 1, \quad u_\xi = 0, \quad u_\theta = 0, \quad p = 1 - \xi^4.$$

We perform the test on two different types of grids as shown in Figures 4.5-4.6. The first is an initially equal-angled polar grid. The second is an initially non-uniform smooth polar grid, for which each internal grid vertex is obtained by a smooth perturbation from an equal-angled polar grid as follows

$$z_{k,l} = \xi_k \cos\theta_l + \epsilon \sin(2\pi\xi_k)\sin(4\theta_l),$$
$$r_{k,l} = \xi_k \sin\theta_l + \epsilon \sin(2\pi\xi_k)\sin(4\theta_l),$$

where $\epsilon = 0.02$. $\xi_k = \frac{k-1}{K}$, $\theta_l = \frac{l-1}{L}\frac{\pi}{2}$, $(z_{k,l}, r_{k,l})$ is the z-r coordinates of the grid points with the sequential indices $(k,l), k = 1, ..., K, l = 2, ..., L$ in the radial and angular directions respectively. K, L represent the number of cells in the above mentioned two directions.

Free boundary condition is applied on the outer boundary. The grids at $t = 1$ are given in the right figures of Figures 4.5-4.6. In the figures, we use the black points to represent the cells where the positivity-preserving limiter has been enacted at $t = 1$. We can clearly observe the symmetry-preserving property of the scheme on the equal-angled polar grid. The error and accuracy of the scheme on these two kinds of grids at $t = 1$ are listed in Tables 4.3-4.4. Due to the numerical singularity, accuracy degeneracy phenomena may happen at the origin and the free outer boundary, thus we remove several points in these two areas to avoid the influence of boundary conditions in the convergence results. Here we measure the error and accuracy on the interval $[\xi_{\frac{1}{10}K+1}, \xi_{\frac{9}{10}K}] \times [\theta_1, \theta_L]$. The time-averaged percentage of the cells in which the positivity-preserving limiter has been performed is also listed in the tables. Here we take the result of the one-dimensional third order positivity-preserving Lagrangian scheme in the spherical coordinate with 10,000 cells as our reference solution. From the tables, we can see the expected second order accuracy in both L_1 and L_∞ norms

for all the evolved conserved variables on both kinds of grids.

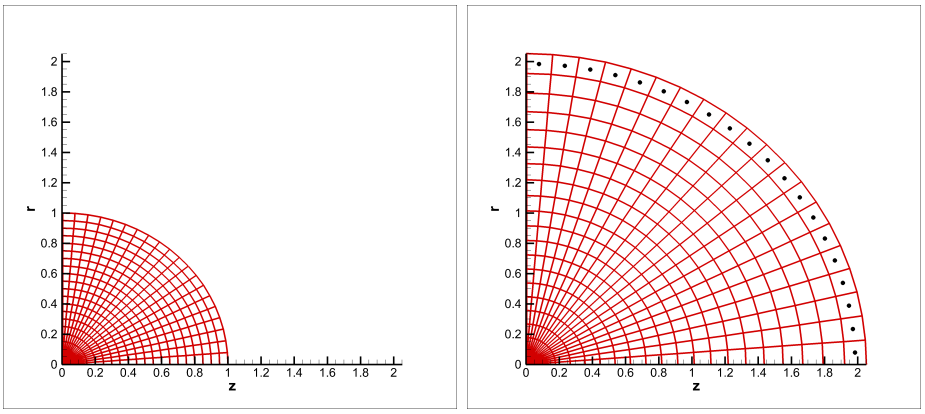

Figure 4.5: The equal-angled polar grid of the free expansion problem with 20×20 cells. Left: initial grid; Right: grid at $t = 1$. The black points in the figure represent the cells where the positivity-preserving limiter has been enacted at $t = 1$.

Table 4.3: Errors of the scheme in 2D cylindrical coordinates for the free expansion problem using $K \times L$ initially equal-angled polar grid cells

$K = L$	Norm	Density	order	Momentum	order	Energy	order	limited cells(%)
10	L_1	0.15E-2		0.19E-2		0.20E-2		8.15
	L_∞	0.89E-2		0.29E-2		0.68E-2		
20	L_1	0.62E-3	1.27	0.45E-3	2.12	0.42E-3	2.22	4.06
	L_∞	0.21E-2	2.08	0.75E-3	1.94	0.16E-2	2.12	
40	L_1	0.18E-3	1.81	0.11E-3	1.96	0.11E-3	1.93	2.09
	L_∞	0.41E-3	2.44	0.17E-3	2.19	0.28E-3	2.58	
80	L_1	0.44E-4	2.03	0.26E-4	2.16	0.27E-4	2.07	1.09
	L_∞	0.10E-3	2.00	0.42E-4	1.97	0.69E-4	2.02	

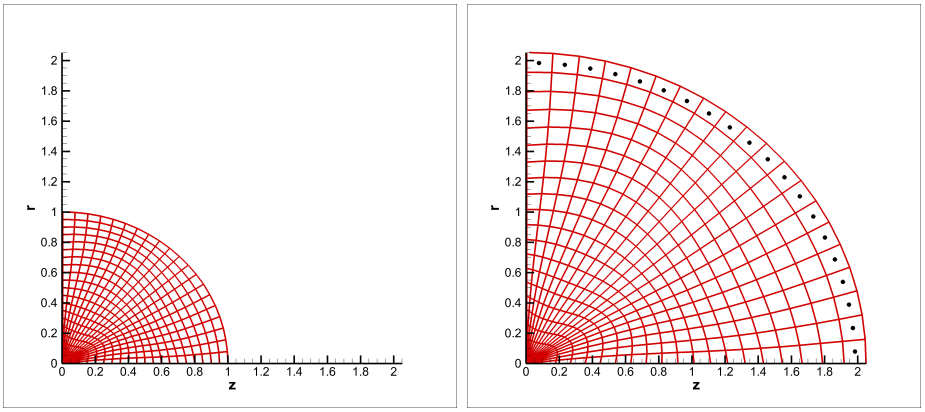

Figure 4.6: The smooth non-equal-angled polar grid of the free expansion problem with 20×20 cells. Left: the initial grid; Right: the grid at $t = 1$. The black points in the figure of the grid represent the cells where the positivity-preserving limiter has been enacted at $t = 1$.

Table 4.4: Errors of the scheme in 2D cylindrical coordinates for the free expansion problem using $K \times L$ initially smooth non-equal-angled polar grid cells

$K = L$	Norm	Density	order	Momentum	order	Energy	order	limited cells(%)
10	L_1	0.15E-2		0.20E-2		0.19E-2		7.97
	L_∞	0.11E-1		0.44E-2		0.79E-2		
20	L_1	0.62E-3	1.26	0.46E-3	2.07	0.44E-3	2.14	3.93
	L_∞	0.23E-2	2.23	0.13E-2	1.81	0.17E-2	2.20	
40	L_1	0.18E-3	1.76	0.13E-3	1.88	0.12E-3	1.86	2.02
	L_∞	0.41E-3	2.45	0.29E-3	2.12	0.29E-3	2.55	
80	L_1	0.47E-4	1.97	0.33E-4	1.95	0.34E-4	1.83	1.05
	L_∞	0.11E-3	1.94	0.82E-4	1.83	0.86E-4	1.78	

Example 2 (The spherical Sedov problem in a cylindrical coordinate system on the polar grid [17]).

The spherical Sedov blast wave problem in a cylindrical coordinate system is a commonly used example of a diverging shock wave. The initial computational domain is a $\frac{1}{4}$-circle region defined in the polar coordinates by $[0, 1.125] \times [0, \pi/2]$. The initial condition is,

$$\rho = 1, \quad u_\xi = 0, \quad u_\theta = 0.$$

The specific internal energy is 10^{-14} except in the cells connected to the origin where they share a total value of 0.2468. Reflective boundary condition is applied on the outer boundary. The analytical solution is a shock with a peak density of 4 at radius unity at time unity. The

final grid and the surface of density and pressure obtained by the second order scheme with 40×40 cells are displayed in Figures 4.7. We observe the expected symmetry in the plots of grid, density and pressure. The density and pressure as a function of ξ at all the cell centers on 20×20, 40×40 and 80×80 grids are shown in Figure 4.8 respectively. In the figures, we observe that the values of density and pressure with the same ξ coincide with each other completely, which clearly demonstrates the symmetry-preserving property of the scheme. The shock position, peak density and pressure agree with the analytical solutions better with the refinement of grid, which verifies the good performance of the scheme in symmetry-preserving, positivity-preserving, non-oscillation and accuracy properties. The centers of all the cells where the positivity-preserving limiter has been effective with the time marching are shown in the right figure of Figure 4.8, which shows that the limiter always acts along the front of the shock wave in this test.

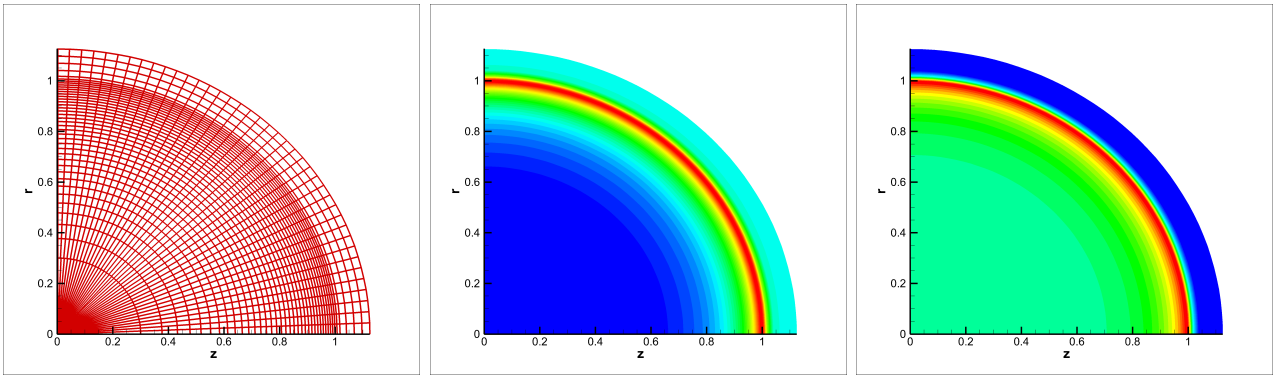

Figure 4.7: The results of the Sedov problem on an equal-angled polar grid with 40×40 cells at $t = 1$. Left: the grid; Middle: density contour; Right: pressure contour.

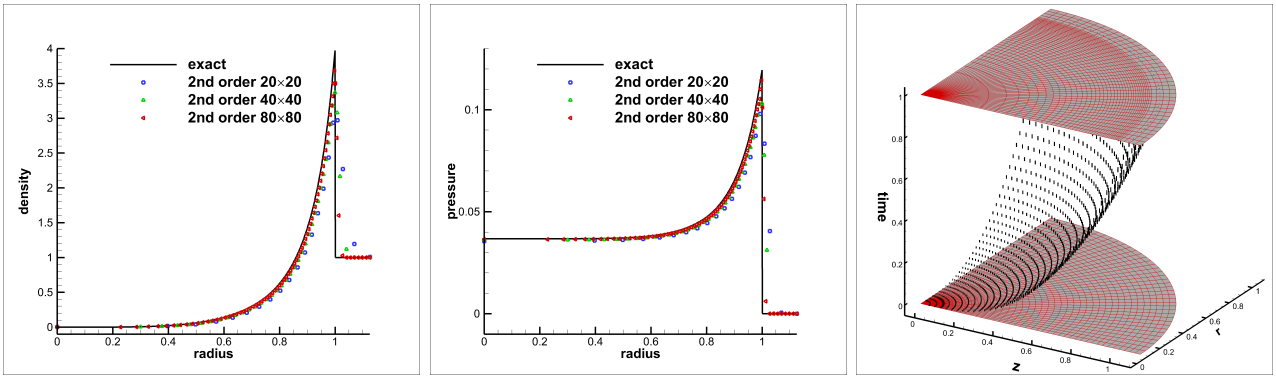

Figure 4.8: The results of the Sedov problem on an equal-angled polar grid at $t = 1$. Left: ρ vs ξ at all the cell centers on 20×20, 40×40 and 80×80 grids respectively. Middle: p vs ξ at all the cell centers on 20×20, 40×40 and 80×80 grids respectively. Solid line: exact solution; Symbols: second order scheme. Right: Black points: the cell centers where the positivity-preserving limiter has been enacted with the time marching on the 40×40 grid, Red lines: grids at $t = 0$ and $t = 1$.

Example 3 (Implosion problem of Lazarus [11]).

In this self-similar implosion problem, initially a sphere of unit radius has the following condition,

$$\rho = 1, \quad u_\xi(t) = \frac{-\alpha f}{(1 - ft)^{1-\alpha}}, \quad u_\theta(t) = 0, \quad e = 10^{-14},$$

where $\alpha = 0.6883545$, $f = 1 - \varepsilon t - \delta t^3$, $\varepsilon = 0.185$, $\delta = 0.28$.

We test the problem on an equal-angled polar grid of 200×30 cells in the initial computational domain $[0, 1] \times [0, \pi/2]$ defined in the polar coordinates. Free boundary condition is applied on the outer boundary. The numerically converged result computed using a one-dimensional third-order Lagrangian code in the spherical coordinate with 10,000 cells is used as a reference solution. We display the results of the second order scheme in Figures 4.9-4.10. In the plots of the grid, density contour and pressure contour, we notice the expected symmetry. In the plot of density and pressure as a function of ξ at all the cell centers, we observe the non-oscillatory, symmetry-preserving and positivity-preserving properties of the scheme. The centers of all the cells where the positivity-preserving limiter has been performed with the time marching are shown in the right figure of Figure 4.10. In the figure, we could see that the limiter acts near the shock front and the outer boundary in this test.

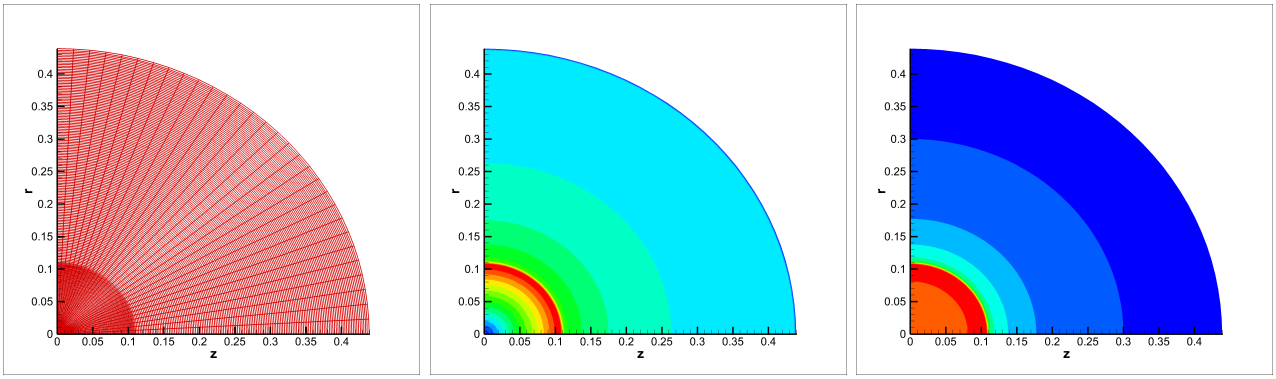

Figure 4.9: The results of the Lazarus problem on an equal-angled polar grid with 200×30 cells at $t = 0.8$. Left: grid; Middle: density contour; Right: pressure contour.

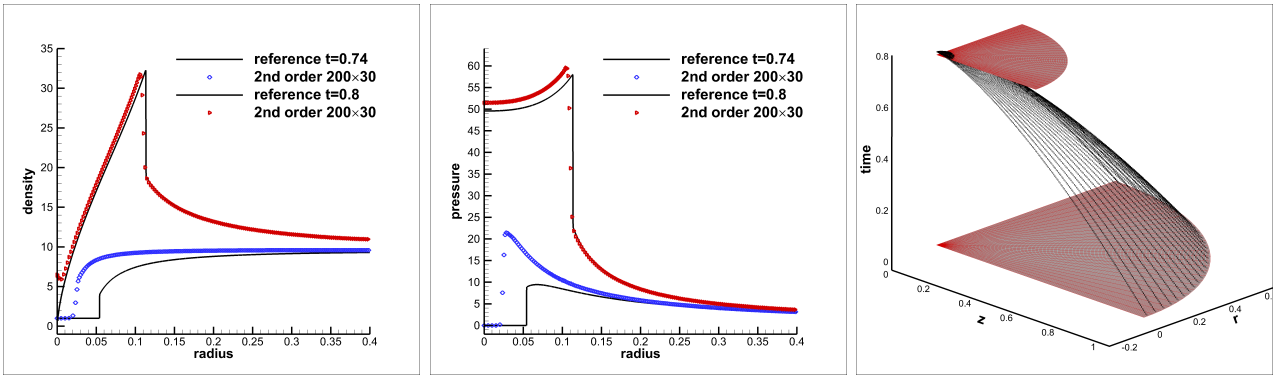

Figure 4.10: The results of the Lazarus problem on an equal-angled polar grid with 200×30 cells at $t = 0.74$, 0.8. Left: ρ vs ξ at all the cell centers; Middle: p vs ξ at all the cell centers. Solid line: reference solution; Symbols: second order scheme. Right: Black points: the cell centers where the positivity-preserving limiter has been enacted with the time marching, Red lines: the grids at $t = 0$ and $t = 0.74$.

Example 4 (The Noh problem in a cylindrical coordinate system on the polar grid [15]).

In this test case, the perfect gas has the following initial condition,

$$\rho = 1, \quad u_\xi = -1, \quad u_\theta = 0, \quad e = 10^{-13}.$$

The equal-angled polar grid is applied in the $\frac{1}{4}$-circle computational domain defined in the polar coordinates by $[0, 1] \times [0, \pi/2]$. Free boundary condition is applied on the outer boundary. The shock is generated by bringing the cold gas to rest at the origin. The analytical post shock density is 64 and the shock speed is 1/3. Figure 4.11 shows the results of the second

order scheme including the final grid, density contour and pressure contour with 100×20 cells at $t = 0.6$. The density and pressure as a function of ξ at all the cell centers on 25×5, 50×10 and 100×20 grids are given in Figure 4.12 respectively, where we observe the results are convergent, symmetric, positivity-preserving and non-oscillatory near the shock.

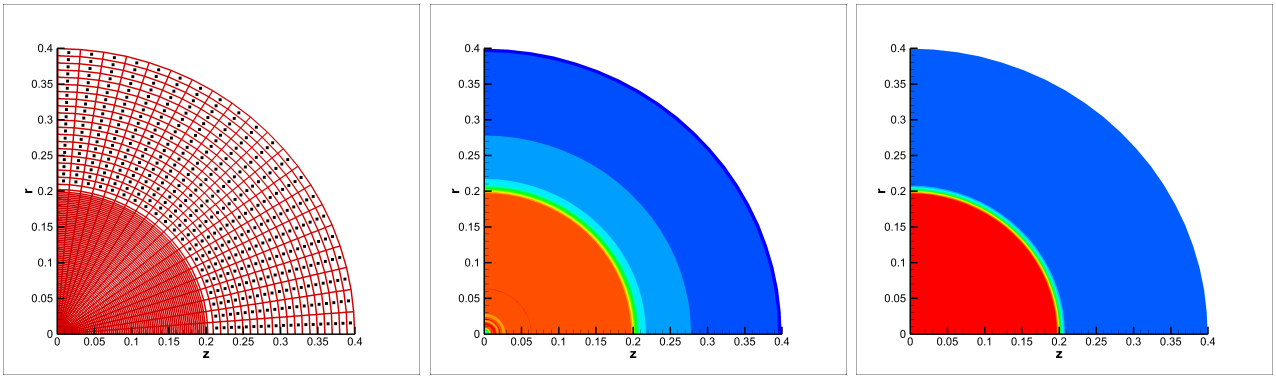

Figure 4.11: The results of the Noh problem on an equal-angled polar grid with 100×20 cells at $t = 0.6$. Left: the grid; Middle: density contour; Right: pressure contour. The black points in the figure of the grid represent the cells where the positivity-preserving limiter has been enacted.

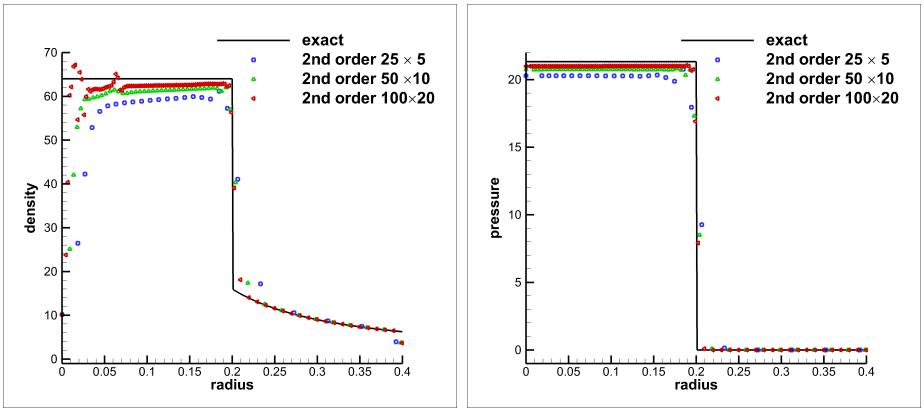

Figure 4.12: The results of the Noh problem on equal-angled polar grids with 25×5, 50×10 and 100×20 cells respectively at $t = 0.6$. Left: ρ vs ξ at all the cell centers. Right: p vs ξ at all the cell centers. Solid line: exact solution; Symbols: numerical solution.

Example 5 (Spherical Sedov problem on the Cartesian grid).

The spherical symmetry problem simulated on the initially rectangular grid is demonstrated to be much more challenging for a Lagrangian scheme due to the shock direction

being not aligned with the grid line. In this example, we test the spherical Sedov blast wave problem in a cylindrical coordinate system on the initially rectangular grid. The initial computational domain is a 1.125×1.125 square consisting of 30×30 uniform cells. Its initial condition is

$$\rho = 1, \quad u_z = 0, \quad u_r = 0.$$

The specific internal energy e is 10^{-14} except in the cell connected to the origin where it has a value of 0.2468. Reflective boundary condition is applied on the right and top boundaries. Figures 4.13-4.14 show the results of our second order scheme (3.14) with (3.10)-(3.13). From the figures, we can observe the results of our second order scheme are positivity-preserving and roughly symmetric even on this non-polar grid.

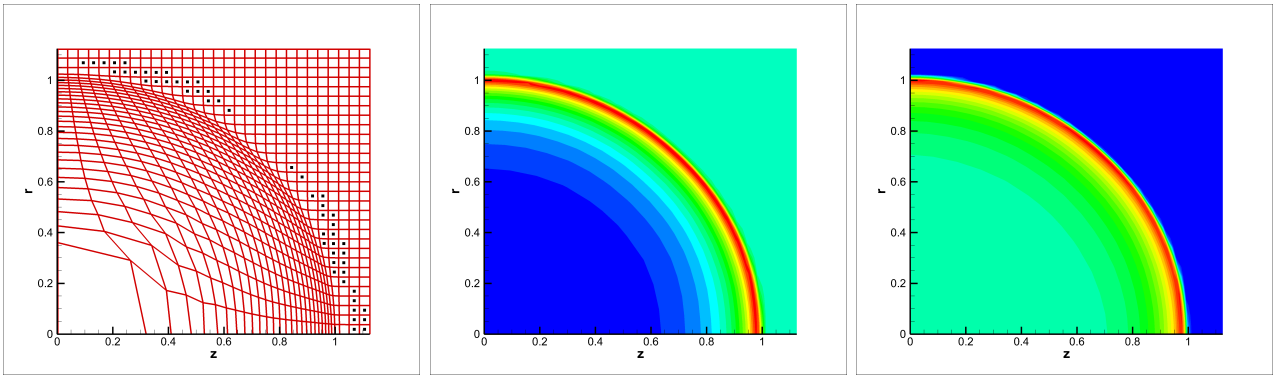

Figure 4.13: The results of the Sedov problem on a Cartesian grid with 30×30 cells at $t = 1$. Left: grid; Middle: density contour ; Right: pressure contour. The black points in the figure of grid represent the cells where the positivity-preserving limiter has been enacted.

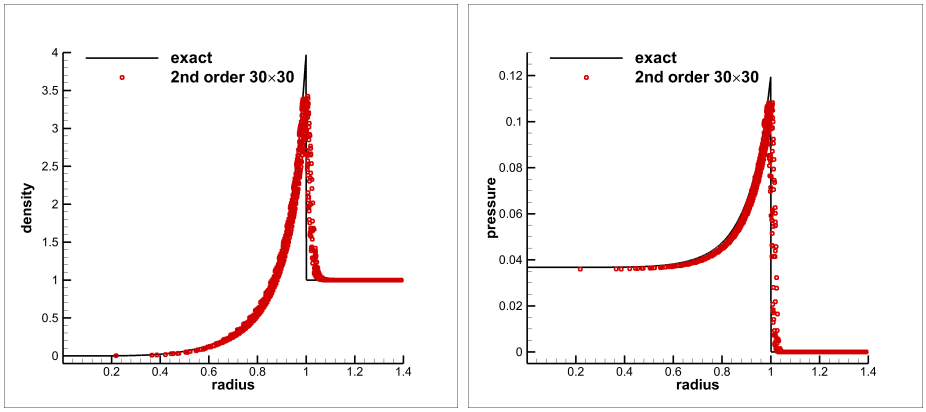

Figure 4.14: The results of the Sedov problem on a Cartesian grid with 30×30 cells at $t = 1$. Left: ρ vs ξ at all the cell centers; Right: p vs ξ at all the cell centers. Solid line: exact solution; Symbols: second order scheme.

Example 6 (Spherical Noh problem on the Cartesian grid [15]).

In this example, we test the spherical Noh implosion problem on a Cartesian grid to verify the robustness of the scheme. The initial domain is $[0, 1] \times [0, 1]$. The initial state of the fluid is $(\rho, u_\xi, u_\theta, e) = (1, -1, 0, 10^{-13})$. Free boundary condition is applied on the right and top boundaries. The analytical solution is the same as that in Example 4. Figures 4.15-4.16 show the results of the second order scheme with 30×30 initially uniform rectangular cells at $t = 0.6$. From these figures, we can see that there is no grid distortion along the axes, the spherical symmetry of the shock front is preserved well, the shock position is correct and the positivity of density and pressure is maintained very well, which demonstrate the robustness of the scheme on the Cartesian grid.

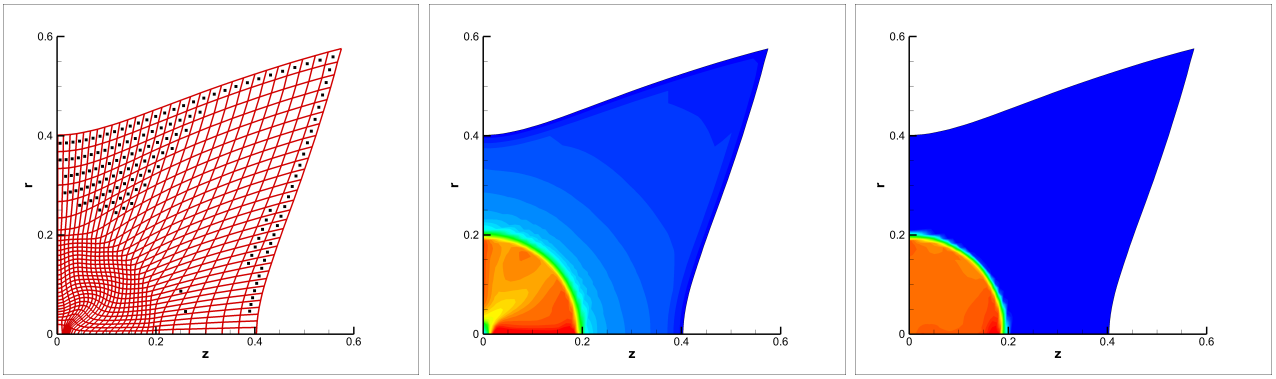

Figure 4.15: The results of the Noh problem on a Cartesian grid with 30×30 cells at $t = 0.6$. Left: the grid; Middle: density contour; Right: pressure contour. The black points in the figure of the grid represent the cells where the positivity-preserving limiter has been enacted at $t = 0.6$.

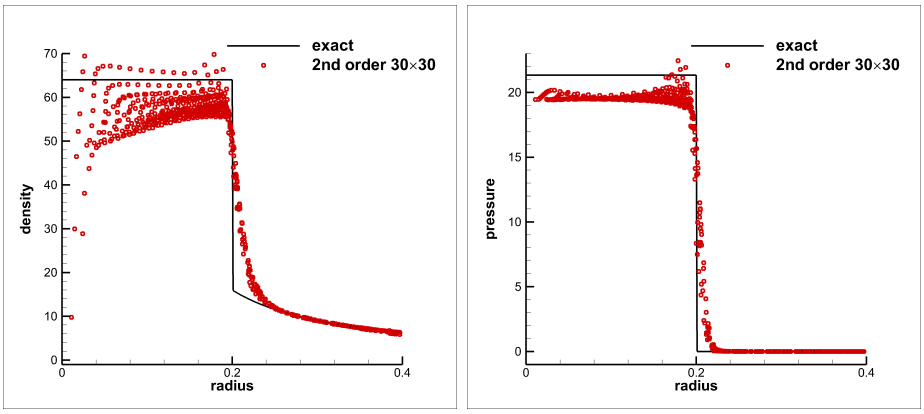

Figure 4.16: The results of the Noh problem on a Cartesian grid with 30×30 cells at $t = 0.6$. Left: ρ vs ξ at all the cell centers. Right: p vs ξ at all the cell centers. Solid line: exact solution; Symbols: numerical solution.

5 Conclusion

In this paper, we focus on the methodology to design positivity-preserving and symmetry p-reserving Lagrangian schemes in one- and two- dimensional cylindrical coordinates for solving compressible Euler equations with general equations of state. Firstly, we develop the first order positivity-preserving Lagrangian scheme and high order positivity-preserving Lagrangian scheme by using positivity-preserving limiter for Euler equations in one-dimensional cylindrical coordinates, which are performed based on the two-state Riemann solver [13, 18]. Then

for the two-dimensional cylindrical coordinate case, we consider the preservation of positivity and symmetry simultaneously (the spherical symmetry is considered when computed on an equal-angle-zoned initial grid). To achieve this goal, we need to discuss the mutual impact of these two properties on each other, then make a balance between them. The main idea is to perform the area based reconstruction in a local ξ-θ coordinate [6], and perform the positivity-preserving limiter also for such reconstructions and in such local coordinates. Our schemes also maintain other good properties such as conservation for mass, momentum and total energy and the geometric conservation law. Several numerical examples in cylindrical coordinates are given to demonstrate the good performance of the schemes in terms of accuracy, positivity-preserving, symmetry-preserving, non-oscillation and robustness properties.

Appendix A. Two-state Riemann solver

Let $\mathsf{U}_L = (\rho_L, u_L, E_L)^\top$ and $\mathsf{U}_R = (\rho_R, u_R, E_R)^\top$ be the initial left and right states, then the left and right intermediate states as U_-^* and U_+^* can be determined by the Rankine-Hugoniot relations

$$\begin{cases} \frac{1}{\rho_-^*} = \frac{1}{\rho_L} + \frac{u_-^* - u_L}{\widetilde{z}_L} \\ u_-^* = u_L - \frac{p_-^* - p_L}{\widetilde{z}_L} \\ E_-^* = E_L - \frac{p_-^* u_-^* - p_L u_L}{\widetilde{z}_L} \end{cases} \quad \text{and} \quad \begin{cases} \frac{1}{\rho_+^*} = \frac{1}{\rho_R} - \frac{u_+^* - u_R}{\widetilde{z}_R} \\ u_+^* = u_R + \frac{p_+^* - p_R}{\widetilde{z}_R} \\ E_+^* = E_R + \frac{p_+^* u_+^* - p_R u_R}{\widetilde{z}_R} \end{cases}, \tag{A.1}$$

where $\widetilde{z}_L$ and $\widetilde{z}_R$ are the local approximations of the acoustic impedance. According to the continuity of the pressure and the velocity across a contact discontinuity, we can obtain the associated numerical fluxes

$$u_-^* = u_+^* = u^* = \frac{\widetilde{z}_L u_L + \widetilde{z}_R u_R}{\widetilde{z}_L + \widetilde{z}_R} - \frac{1}{\widetilde{z}_L + \widetilde{z}_R}(p_R - p_L), \tag{A.2a}$$

$$p_-^* = p_+^* = p^* = \frac{\widetilde{z}_L p_R + \widetilde{z}_R p_L}{\widetilde{z}_L + \widetilde{z}_R} - \frac{\widetilde{z}_L \widetilde{z}_R}{\widetilde{z}_L + \widetilde{z}_R}(u_R - u_L). \tag{A.2b}$$

Appendix B. A proof for Lemma 3.3

We notice that the condition (3.37) can be rewritten as

$$\sum_{q \in Q_c \setminus \underline{p}} r_q^c l_q^c \pi_q^{c,a} \boldsymbol{n}_q^c = -r_{\underline{p}}^c l_{\underline{p}}^c \pi_{\underline{p}}^{c,a} \boldsymbol{n}_{\underline{p}}^c. \tag{B.1}$$

To make $\hat{\mathcal{F}}_{\underline{p}}$ defined in (3.38) mimicking the first order scheme (3.14), we introduce

$$\pi_{\underline{p}}^{q} = \begin{cases} \pi_{\underline{p}}^{c}, & \text{if } q = \underline{p} \\ \pi_{\underline{p}}^{c,a}, & \text{otherwise} \end{cases} \tag{B.2}$$

where $\pi_{\underline{p}}^{q}$ is also some artificial pressure and its corresponding artificial velocity is denoted as $\mathbf{u}_{\underline{p}}^{q}$. Then based on (B.1), $\hat{\mathcal{F}}_{\underline{p}}$ for arbitrary p finally reads

$$\hat{\mathcal{F}}_{\underline{p}} = \begin{pmatrix} \dfrac{m_c}{\omega V_c^{n+1}} \\ u_{\underline{p}}^{c,z} - \dfrac{\Delta t^n}{\omega_{\underline{p}} m_c} \displaystyle\sum_{q\in Q_c} r_q^c l_q^c \pi_{\underline{p}}^q n_q^{c,z} \\ u_{\underline{p}}^{c,r} - \dfrac{\Delta t^n}{\omega_{\underline{p}} m_c} \displaystyle\sum_{q\in Q_c} r_q^c l_q^c \pi_{\underline{p}}^q n_q^{c,r} + \dfrac{\Delta t^n}{\omega_{\underline{p}} m_c}(\dfrac{1}{8}A_c)P_s \\ E_{\underline{p}}^{c} - \dfrac{\Delta t^n}{\omega_{\underline{p}} m_c} \displaystyle\sum_{q\in Q_c} r_q^c l_q^c \pi_{\underline{p}}^q \boldsymbol{n}_q^c \cdot \mathbf{u}_{\underline{p}}^q \end{pmatrix}. \tag{B.3}$$

Hence $\hat{\mathcal{F}}_{\underline{p}}$ is nothing but the first order scheme defined in (3.14), so is $\hat{\mathcal{F}}_{\overline{p}}$.

If we apply the formula in (3.10) to the artificial numerical flux $\pi_{\underline{p}}^{q}$, we can get

$$\begin{aligned} \sum_{q\in Q_c} r_q^c l_q^c \pi_{\underline{p}}^q \boldsymbol{n}_q^c &= \sum_{q\in Q_c} r_q^c l_q^c (p_{\underline{p}}^c - \widetilde{z}_{\underline{p}}^q (\boldsymbol{u}_p - \mathbf{u}_{\underline{p}}^q)\cdot \boldsymbol{n}_q^c)\boldsymbol{n}_q^c \\ &= p_{\underline{p}}^c \sum_{q\in Q_c} r_q^c l_q^c \boldsymbol{n}_q^c - \sum_{q\in Q_c} r_q^c l_q^c \widetilde{z}_{\underline{p}}^q (\boldsymbol{u}_p - \mathbf{u}_{\underline{p}}^q)\cdot \boldsymbol{n}_q^c \boldsymbol{n}_q^c \\ &= A_c p_{\underline{p}}^c \boldsymbol{e}_r - \sum_{q\in Q_c} r_q^c l_q^c \widetilde{z}_{\underline{p}}^q (\boldsymbol{n}_q^c \otimes \boldsymbol{n}_q^c)(\boldsymbol{u}_p - \mathbf{u}_{\underline{p}}^q) \\ &= A_c p_{\underline{p}}^c \boldsymbol{e}_r - \sum_{q\in Q_c} M_{\underline{p}c}^q (\boldsymbol{u}_p - \mathbf{u}_{\underline{p}}^q) \end{aligned}$$

where $\boldsymbol{e}_r = (0,1)^\top$, $M_{\underline{p}c}^q = r_q^c l_q^c \widetilde{z}_{\underline{p}}^q (\boldsymbol{n}_q^c \otimes \boldsymbol{n}_q^c)$. Making use of (3.38) and (B.1), the last relation above can be rewritten as

$$\begin{aligned} (\pi_{\underline{p}}^c - \pi_{\underline{p}}^q) r_{\underline{p}}^c l_{\underline{p}}^c \boldsymbol{n}_{\underline{p}}^c &= A_c p_{\underline{p}}^c \boldsymbol{e}_r - M_{\underline{p}c}^{\underline{p}} (\boldsymbol{u}_p - \boldsymbol{u}_{\underline{p}}^c) - \sum_{q\in Q_c\setminus \underline{p}} M_{\underline{p}c}^q (\mathbf{u}_c - \boldsymbol{u}_{\underline{p}}^c) \\ &= A_c p_{\underline{p}}^c \boldsymbol{e}_r - M_{\underline{p}c}^{\underline{p}} (\boldsymbol{u}_p - \boldsymbol{u}_{\underline{p}}^c) - M_c^{\underline{p}} (\mathbf{u}_c - \boldsymbol{u}_{\underline{p}}^c) \end{aligned}$$

where $M_c^{\underline{p}} = \displaystyle\sum_{q\in Q_c\setminus \underline{p}} M_{\underline{p}c}^q$. Finally, by means of (3.10), we can define the artificial pressure $\pi_{\underline{p}}^{c,a}$ as

$$\pi_{\underline{p}}^{c,a} r_{\underline{p}}^c l_{\underline{p}}^c \boldsymbol{n}_{\underline{p}}^c = p_{\underline{p}}^c r_{\underline{p}}^c l_{\underline{p}}^c \boldsymbol{n}_{\underline{p}}^c + M_c^{\underline{p}} (\mathbf{u}_c - \boldsymbol{u}_{\underline{p}}^c) - A_c p_{\underline{p}}^c \boldsymbol{e}_r, \tag{B.4}$$

then the condition (B.1) makes us to determine the artificial velocity $\mathbf{u}_c$ uniquely

$$\mathbf{u}_c = \left(\sum_{p \in p(c)} (M_c^{\underline{p}} + M_c^{\overline{p}}) \right)^{-1} \sum_{p \in p(c)} \left((M_c^{\underline{p}} + M_c^{\overline{p}}) \boldsymbol{u}_p - p_{\underline{p}}^c r_{\underline{p}}^c l_{\underline{p}}^c \boldsymbol{n}_{\underline{p}}^c - p_{\overline{p}}^c r_{\overline{p}}^c l_{\overline{p}}^c \boldsymbol{n}_{\overline{p}}^c + A_c (p_{\underline{p}}^c + p_{\overline{p}}^c) \boldsymbol{e}_r \right). \tag{B.5}$$

References

[1] P. Battern, N. Clarke, C. Lambert, D. Causon. On the choice of wavespeeds for the HLLC Riemann solver. SIAM J. Sci. Comput. 18 (1997) 1553-1570.

[2] J. Cheng, C.-W. Shu. A third order conservative Lagrangian type scheme on curvilinear meshes for the compressible Euler equations. Commun. Comput. Phys. 4 (2008) 1008-1024.

[3] J. Cheng, C.-W. Shu. A cell-centered Lagrangian scheme with the preservation of symmetry and conservation properties for compressible fluid flows in the two-dimensional cylindrical geometry. J. Comput. Phys. 229 (2010) 7191-7206.

[4] J. Cheng, C.-W. Shu. Improvement on spherical symmetry in two-dimensional cylindrical coordinates for a class of control volume Lagrangian schemes. Commun. Comput. Phys. 11 (2012) 1144-1168.

[5] J. Cheng, C.-W. Shu. Positivity-preserving Lagrangian scheme for multi-material compressible flow. J. Comput. Phys. 257 (2014) 143-168.

[6] J. Cheng, C.-W. Shu. Second order symmetry-preserving conservative Lagrangian scheme for compressible Euler equations in two-dimensional cylindrical coordinates. J. Comput. Phys. 272 (2014) 245-265.

[7] J. K. Dukowicz. A general non-interactive Riemann solver for Godunov's method. J. Comput. Phys. 61 (1984) 119-137.

[8] B. Einfeldt, C. D. Munz, P. L. Roe, B. Sjögreen. On Godunov-type methods near low densities. J. Comput. Phys. 92 (1991) 273-295.

[9] G. Gallice. Positive and entropy stable Godunov-type schemes for gas dynamics and MHD equations in Lagrangian or Eulerian coordinates. Numer. Math. 94 (2003) 673-713.

[10] A. Harten, B. Engquist, S. Osher, S. Chakravarthy. Uniformly high order essentially non-oscillatory schemes, III. J. Comput. Phys. 71 (1987) 231-303.

[11] R. Lazarus. Self-similar solutions for converging shocks and collapsing cavities. SIAM J. Numer. Anal. 18 (1981) 316-371.

[12] P.-H. Maire. A high-order cell-centered Lagrangian scheme for compressible fluid flows in two-dimensional cylindrical geometry. J. Comput. Phys. 228 (2009) 6882-6915.

[13] P.-H. Maire. Contribution to the numerical modeling of Inertial Confinement Fusion, Habilitation à Diriger des Recherches, Bordeaux University, 2011, available at http://tel.archives-ouvertes. fr/docs/00/58/97/58/PDF/hdr_main.pdf.

[14] C. D. Munz. On Godunov-type schemes for Lagrangian gas dynamics. SIAM J. Numer. Anal. 31 (1994) 17-42.

[15] W.F. Noh. Errors for calculations of strong shocks using an artificial viscosity and an artificial heat flux. J. Comput. Phys. 72 (1987) 78-120.

[16] B. Perthame, C.-W. Shu. On positivity preserving finite volume schemes for Euler equations. Numer. Math. 73 (1996) 119-130.

[17] L.I. Sedov. Similarity and Dimensional Methods in Mechanics. Academic Press, New York, 1959.

[18] F. Vilar, C.-W. Shu, P.-H. Maire. Positivity-preserving cell-centered Lagrangian Schemes for multi-material compressible flows: From first-order to high-orders, Part I: The one-dimensional case. J. Comput. Phys. 312 (2016) 385-415.

[19] F. Vilar, C.-W. Shu, P.-H. Maire. Positivity-preserving cell-centered Lagrangian Schemes for multi-material compressible flows: From first-order to high-orders, Part I-I: The two-dimensional case. J. Comput. Phys. 312 (2016) 416-442.

[20] X. Zhang, C.-W. Shu. On positivity-preserving high order discontinuous Galerkin schemes for compressible Euler equations on rectangular meshes. J. Comput. Phys. 229 (2010) 8918-8934.

[21] X. Zhang, C.-W. Shu. Positivity-preserving high order discontinuous Galerkin schemes for compressible Euler equations with source term. J. Comput. Phys. 230 (2011) 1238-1248.

[22] X. Zhang, C.-W. Shu. Maximum-principle-satisfying and positivity-preserving high order schemes for conservation laws: Survey and new developments. Pro. R. Soc. A. 467 (2011) 2752-2776.